Mon. Not. R. Astron. Soc. **347,** 691–719 (2004)

On the mass-to-light ratio and the initial mass function in disc galaxies

L. Portinari,[1⋆] J. Sommer-Larsen[1⋆] and R. Tantalo[2⋆]

[1] *Theoretical Astrophysics Centre, Juliane Maries Vej 30, DK-2100 Copenhagen Ø, Denmark*
[2] *Dipartimento di Astronomia, Università di Padova, Vicolo dell'Osservatorio 2, I-35122 Padova, Italy*

Accepted 2003 September 12. Received 2003 September 7; in original form 2003 July 4

ABSTRACT

A low mass-to-light (M/L) ratio for the stellar component of spiral galaxies ($M/L \lesssim 1$ in the I band) is advocated by various dynamical arguments and by recent cosmological simulations of the formation of these systems. We discuss this possibility by means of chemo-photometric models for galactic discs, adopting different initial mass functions (IMFs). We show that a number of 'bottom-light' initial mass functions (namely, with less mass locked in low-mass stars than the standard Salpeter IMF), suggested independently in recent literature, do imply M/L ratios as low as mentioned above, at least for late-type spirals (Sbc/Sc). This conclusion still holds when the bulge contribution to mass and light is included. We also predict the typical stellar M/L ratio, and correspondingly the zero-point of the Tully–Fisher relation, to vary considerably with Hubble type (approximately 0.5–0.7 mag in the red bands, from Sa to Sc type).

For some of the bottom-light IMFs considered, the efficiency of metal production tends to exceed what is typically estimated for spiral galaxies. Suitable tuning of the IMF mass limits, post-supernova fallback of metals on to black holes or metal outflows must then be invoked, to reproduce the observed chemical properties of disc galaxies.

In the appendix we provide M/L–colour relations to estimate the stellar M/L ratio of a galaxy on the basis of its colours, for several IMFs.

Key words: stars: luminosity function, mass function – galaxies: evolution – galaxies: spiral.

1 INTRODUCTION

Present cosmological simulations of the formation of disc galaxies within the cold dark matter hierarchical scenario suffer from the angular momentum problem (Navarro, Frenk & White 1995). Suggested ways out of this problem include early energy injection from stellar feedback (Sommer-Larsen, Gelato & Vedel 1999; Thacker & Couchman 2001; Sommer-Larsen, Götz & Portinari 2003) or warm dark matter cosmology (Sommer-Larsen & Dolgov 2001). Such N-body–smoothed particle hydrodynamics (SPH) simulations not only improve significantly on the angular momentum problem, but also compare successfully with the observed Tully–Fisher (TF) relation, *provided* the mass-to-light (M/L) ratio of the stellar component is low (Sommer-Larsen & Dolgov 2001; Sommer-Larsen et al. 2003): in the I band, the inferred $M/L_I \sim 0.8$ (Fig. 1). However, in cosmological simulations the need for a low baryonic M/L ratio may be partly due to the too dense cores of dark matter haloes: in simulated galaxies, dark matter is more concentrated and dynamically dominant in the central regions, than estimated from rotation curves (Navarro & Steinmetz 2000a,b; de Blok, McGaugh & Rubin 2001a; de Blok et al. 2001b; Eke, Navarro & Steinmetz 2001; Salucci 2001; Salucci & Borriello 2001; Bottema 2002; de Blok & Bosma 2002; Marchesini et al. 2002; Abadi et al. 2003).

The suggestion of a low stellar M/L ratio is nevertheless reinforced by a simple estimate of the stellar mass of our Galaxy, based on the local stellar density and on a plausible density profile for the disc (Sommer-Larsen & Dolgov 2001). The stellar mass obtained in this way for the Milky Way is of the order of 5×10^{10} $M_\odot$, and if our Galaxy is to lie on the observed TF relation together with other spirals, its M/L_I ratio must be around 0.75 (see Fig. 1). Considering all uncertainties, Sommer-Larsen & Dolgov (2001) estimate for the *total* baryonic matter in the Milky Way (inclusive of stars, gas and stellar remnants) $M/L_I = 0.87 \pm 0.57$.

Similar conclusions can be drawn from the Sb galaxy NGC 2841: estimates of its disc mass range between $5\ h_{50}^{-1} \times 10^{10}$ and $11.7\ h_{75}^{-1} \times 10^{10}$ $M_\odot$[1] and its circular velocity is 317 km s^{-1} (Kent 1987; Benson et al. 2000 and references therein), which also points to $M/L_I \lesssim 0.7$ (Fig. 1). Regarding the zero-point of the Tully–Fisher relation, however, some uncertainties exist and are discussed in Appendix A.

⋆E-mail: lportina@tac.dk (LP); jslarsen@tac.dk (JS-L); tantalo@pd.astro.it (RT)

[1] We indicate with $h = h_{100}$, with h_{50} and with h_{75} the Hubble constant in units of 100, 50 and 75 km s^{-1} Mpc^{-1}.

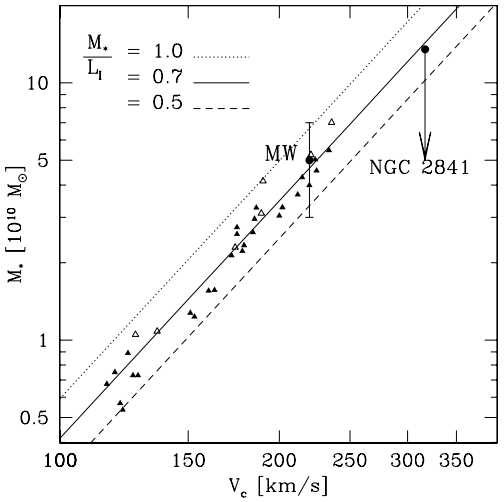

Figure 1. Straight lines, location of the observed Tully–Fisher relation for Sbc–Sc disc galaxies by Giovanelli et al. (1997a,b, $h = 0.65$ adopted here) in the stellar mass versus circular velocity plane, for different assumptions concerning the stellar M/L_I ratio. We also show the location of simulated disc galaxies by Sommer-Larsen et al. (2003, triangles), and of two observed galaxies: the Milky Way and NGC 2841 (the latter rescaled to $h = 0.65$).

An independent indication of a low M/L ratio for the baryonic component of spiral discs relies on stability arguments. Bar instability of isolated discs was one of the reasons to introduce massive dark haloes historically (Ostriker & Peebles 1973); the argument still holds, in the sense that if too much mass is stored in the luminous disc component, strong bars should form. Based on this, Efstathiou, Lake & Negroponte (1982) put an upper limit of $M/L_B \leqslant 1.5\,h$ to the disc M/L ratio, that is $M/L_B \leqslant 1$ for $h = 0.65$.

The M/L ratio of the stellar component is also relevant to the issue as to whether discs are maximal or submaximal, or to what extent the luminous, baryonic mass dominates the dynamics and the rotation curve in the inner regions of the disc. Even under the hypothesis of maximal discs, Bell & de Jong (2001) point out that lower M/L ratios for the stellar component are implied, than those predicted with a Salpeter initial mass function (IMF). And discs may well be submaximal (Bottema 1993, 1997; Courteau & Rix 1999), although this is still much debated (Ratnam & Salucci 2000; Fuchs 2002, 2003a,b; Kranz, Slyz & Rix 2003; Masset & Bureau 2003). For his favoured submaximal disc case, with the luminous component contributing 63 per cent of the rotation curve at maximum, Bottema (2002) suggests a stellar $M/L_I \sim 0.82$ for spirals in the Ursa Major cluster. For the Milky Way itself, a variety of mass models is compatible with available kinematic data (Binney & Merrifield 1998; Dehnen & Binney 1998), so that on this basis no clear discrimination is possible between the maximal or submaximal case; though recent combined results on luminosity and mass distribution, gas flows and microlensing seem to favour a maximal disc (Gerhard 2002).

Two recent, detailed studies of individual spirals also point toward low M/L ratios. A dynamical analysis of the isolated Sc galaxy NGC 4414 indicates an intrinsic stellar $M/L \sim 1$ in the B, V and I bands (Vallejo, Braine & Baudry 2002). For the Sab spiral 2237+0305, Huchra's lens, Trott & Webster (2002) combine dynamical and gravitational lensing constraints to derive $M/L_I \sim 1.1$ for the disc.

In the light of these results, the obvious question arises as to whether M/L ratios that are so low are plausible from the point of view of the stellar content and of the photometric evolution of galaxies; this relies heavily on the stellar IMF of stars in disc galaxies. A standard Salpeter IMF, extended over the typical stellar mass range [0.1–100] $M_\odot$ certainly yields much higher M/L ratios than those mentioned above (see Section 5). On the other hand, there is by now a general consensus that a single-slope power-law IMF over the whole stellar mass range is not adequate for the local nor for other environments. The slope of the IMF appears in fact to become shallower below 1 $M_\odot$, in the local environment (Miller & Scalo 1979; Scalo 1986; Kroupa, Tout & Gilmore 1993; Gould, Bahcall & Flynn 1997; Reid & Gizis 1997; Gould, Flynn & Bahcall 1998; Chabrier 2001) and in globular clusters and in the Galactic Bulge (Piotto & Zoccali 1999; Zoccali et al. 2000). Besides, a turn-over in the regime of brown dwarfs is favoured by recent results (Chabrier 2002). The observed IMF appears to be 'bottom-light' with respect to a single power-law, Salpeter-like IMF (for recent reviews, see Kroupa 2002; Chabrier 2003). From the theoretical point of view, the flattening and turn-over of the IMF at low masses may be related to the Jeans scale (thermal support) and to the scale of magnetic support against gravitational collapse (Larson 1998; Padoan & Nordlund 2002).

In this paper we investigate what kind of IMF is required to obtain a low M/L ratio (say, $\sim$0.8 in the I band) in a typical Sbc–Sc galaxy. We consider different IMFs among those suggested in the literature from a variety of independent studies. For each of these IMFs, we calculate chemical evolution models with infall, metallicity gradients and star formation histories representative of late-type spiral discs; then we compute the corresponding broad-band luminosities by convolving suitable single stellar population (SSP) models with the star formation and metal enrichment histories.

The paper is organized as follows. In Section 2 we discuss which Hubble types and photometric passbands are most relevant for our present analysis of the M/L ratio in galactic discs. In Section 3 we present the various IMFs considered in our chemo-photometric models and in Section 4 the corresponding sets of SSPs. In Section 5 we present simple exponential models with fixed metallicity, to give a first overview of the problem and to discuss the solidity of the predicted M/L ratios with respect to the adopted stellar models and spectral library. In Section 6 we introduce our full chemo-photometric models for disc galaxies, and the corresponding calibration on observational constraints. In Section 7 we present our results on M/L ratios obtained from chemo-photometric models with different IMFs. In Section 8 we add the contribution of the bulge to the global M/L ratio of galaxies. Finally, in Section 9 we outline our summary and conclusions. In Appendix A we discuss observational uncertainties in the zero-point of the TF relation. In Appendix B we provide M/L–colour relations to estimate the stellar M/L ratio of a galaxy on the basis of its colours.

2 FOCUSING ON LATE HUBBLE SPIRAL TYPES

The M/L ratio of the stellar component of a galaxy depends on two basic quantities: the IMF and the star formation history (SFH); the latter sets the relative weight of young, bright and blue stellar populations with respect to old, dim and red ones. The SFH depends on the Hubble type, as clearly indicated by the variation of typical colours along the Hubble sequence (Roberts & Haynes 1994). Hence, the M/L ratio of the stellar mixture is also expected to depend on Hubble type. This effect is indeed observed in the empirical TF relation, where a systematic, negative offset in luminosity is observed when going from Sbc–Sc spirals to Sb to earlier types (Rubin et al. 1985; Giovanelli et al. 1997a); and the offset correlates with the $B - R$ colour as expected from different SFHs in different Hubble types (Kannappan, Fabricant & Franx 2002). Giovanelli et al.

(1997a,b) correct for this morphological dependence, and provide a TF relation (shown in Fig. 1) typical for late spiral types. This allows us to focus on the M/L ratio of Sbc–Sc spirals.

Having selected our fiducial Hubble type, we need to characterize it for the sake of the chemo-photometric models to be developed. The historical, *B*-band-based picture of the Hubble sequence as a sequence of bulge-to-disc ($\mathcal{B}/\mathcal{D}$) ratios is not supported by recent surveys in redder bands; in the *I* or *K* bands, which are better mass tracers, $\mathcal{B}/\mathcal{D}$ correlates fairly weakly with spiral type, and with a huge scatter, thus proving to be a poor morphological indicator (de Jong 1996a; Sommer-Larsen et al. 2003, and references therein; see also Section 8). Kennicutt, Tamblyn & Congdon (1994, hereinafter KTC94) demonstrated that the sequence of spiral types is rather a sequence of different SFHs in the discs themselves, as traced by the so-called *birth rate parameter*

$$b = \frac{\mathrm{SFR}}{\langle \mathrm{SFR} \rangle} \qquad (1)$$

defined as the ratio between the present and past average star formation rate (SFR). KTC94 estimated the b parameter both on the basis of the equivalent width (EW) of the Hα line, and from the ratio between the Hα luminosity (tracer of the present SFR) and the *V*-band luminosity (tracer of the global underlying stellar mass in the disc). The two methods are not completely independent, for EW(Hα) is also a flux ratio between the Hα line and the nearby red continuum (corresponding to the *R* band, roughly), but they give consistent results. From KTC94, the b parameter increases from $b < 0.2$ for Sa–Sab discs, to $b \sim 0.3$–0.4 for Sb discs, to $b \sim 0.8$–1 for Sbc–Sc discs, while the trend breaks down toward later Hubble types, which display more irregular and episodic star formation histories; see also Sommer-Larsen et al. (2003).

Henceforth, in gross terms our chemo-photometric models will be taken to represent typical Sbc–Sc spirals when their SFHs correspond to a b parameter ~ 0.8–1.

2.1 Focusing on the *I* band

In this paper we will mainly discuss the M/L ratio in the *I* band, first because the observational evidence quoted in Section 1, including the fiducial TF, refers to the *I* band. Secondly, red bands such as the *I* band are good mass tracers because they are less sensitive than bluer bands to recent SF episodes, and to metallicity effects (Fig. 2). Thirdly, compared with redder, near-infrared bands, the integrated *I*-band luminosity at intermediate and old ages is not so sensitive to the specific treatment of the asymptotic giant branch (AGB) phase (see Section 5.2). Finally, red bands such as the *I* band are less affected by dust extinction and corresponding corrections. The empirical TF relation by Giovanelli et al., and other observational evidence quoted in the introduction, are already corrected for extinction.

3 THE INITIAL MASS FUNCTION(S)

In this section we discuss the IMFs we have considered in turn in our chemo-photometric models, together with their respective theoretical/observational background. We will present sets of models with three 'power-law IMFs' and three 'exponential IMFs', displayed in Fig. 3. In the following, M will indicate the stellar mass in solar units.

(i) A Salpeter (1955) IMF, extended over the typical stellar mass range [0.1–100] $\mathrm{M}_\odot$:

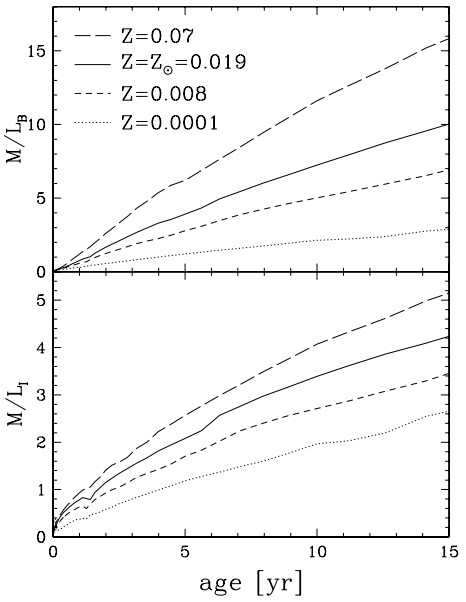

Figure 2. M/L ratio as a function of age for SSPs of different metallicity. Within this wide metallicity range (from $\sim 10^{-2}$ to 3.5 times solar), the M/L ratio in the *I* band varies only by a factor of 2 (lower panel) as opposed to a factor of 5 in the *B* band (upper panel). These M/L ratios are computed from the mass of living stars on the SSP, not including the remnants of more massive, dead stars. The mass of remnants is, however, included in the exponential and chemo-photometric models in the remainder of the paper. This figure is available in colour in the on-line version of the journal on *Synergy*.

$$\Phi(M) = C_\mathrm{s}\, M^{-1.35} \qquad C_\mathrm{s} = 0.1716,$$

where C_s is a normalization coefficient fixed so that the IMF is normalized to unit mass when integrated between the low and high stellar mass ends.

Although the original Salpeter IMF was derived only for stars between 0.4 and 10 $\mathrm{M}_\odot$ and, as mentioned in the introduction (Section 1), there is substantial evidence that a single power law over the entire mass range is not adequate for the observed IMF, this functional form is still widely adopted in the literature and it is useful to include it in the present study, for the sake of comparison with other IMFs.

(ii) The Kroupa (1998) IMF, derived for field stars in the solar neighbourhood and often adopted in chemical evolution models for disc galaxies (e.g. Boissier & Prantzos 1999):

$$\Phi(M) = \begin{cases} C_{kr1} M^{-1/2} & 0.1 < M < 0.5 \\ C_{kr} M^{-1.2} & 0.5 < M < 1 \\ C_{kr} M^{-1.7} & 1 < M < 100 \end{cases}$$

$$C_{kr1} = 0.480 \qquad C_{kr} = 0.295,$$

where C_{kr1} and C_{kr} are fixed so as to guarantee normalization and continuity of the IMF over the range [0.1–100] $\mathrm{M}_\odot$.

This IMF is steeper than the Salpeter one in the high-mass range ($M > 1\,\mathrm{M}_\odot$) but it flattens out progressively at low masses ($M < 1\,\mathrm{M}_\odot$). The steep slope in the high-mass range was actually taken after Scalo (1986). In a more recent determination Kroupa (2001) finds instead a shallower slope of 1.3, close to the Salpeter value, but the steeper Scalo slope is recovered if unresolved binary systems are taken into account (see also Kroupa 2002).

(iii) The Kennicutt (1983) IMF, often advocated as adequate for reproducing the global properties of spiral galaxies (e.g. KTC94,

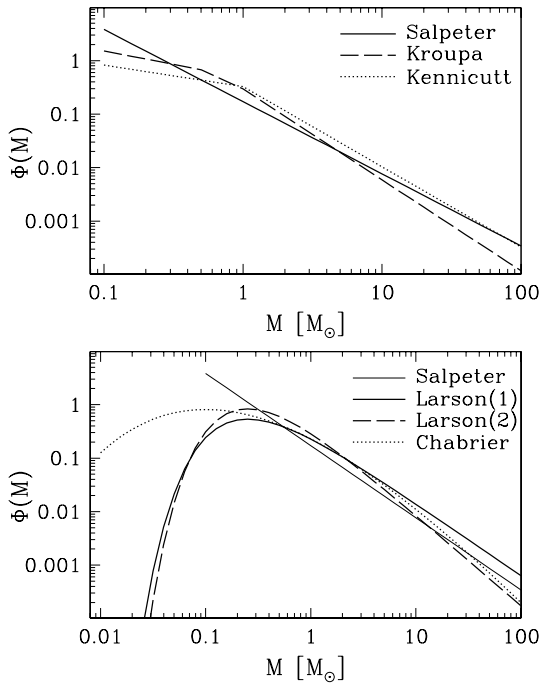

Figure 3. Comparison between the six different IMFs considered in this paper, all normalized to an integrated mass of 1 $M_\odot$. Top panel, the three 'power-law' IMFs (i–iii), defined in the range [0.1–100] $M_\odot$. Bottom panel, the three 'exponential' IMFs (iv–vi), defined in the range [0.01–100] $M_\odot$; Larson (1) and Larson (2) refer to the original and 'modified' Larson IMF, respectively; the Salpeter IMF is also repeated for comparison.

Sommer-Larsen 1996), again with the typical mass range [0.1–100] $M_\odot$,

$$\Phi(M) = \begin{cases} C_{k83} M^{-0.4} & 0.1 < M < 1 \\ C_{k83} M^{-3/2} & 1 < M < 100 \end{cases}$$

$C_{k83} = 0.328$.

This IMF is somewhat shallower in the high-mass range than the local one, as seems to be required to account for the observed Hα luminosities and equivalent widths of external disc galaxies. The flattening below 1 $M_\odot$ is introduced after the observational evidence for the local IMF (see KTC94 for details).

(iv) The Larson (1998) IMF, over the mass range [0.01–100] $M_\odot$, that is down to the substellar regime (which in this case has, however, a negligible contribution to the mass budget):

$$\Phi(M) = C_{L1}\, M^{-1.35} \exp\left(-\frac{M_{L1}}{M}\right)$$

$C_{L1} = 0.317 \qquad M_{L1} = 0.3375.$

This IMF recovers a Salpeter power law at high masses, while at low masses the exponential cut-off produces a characteristic peak mass, or mass scale, $M_\mathrm{p} = M_{L1}/1.35 = 0.25\,M_\odot$ in agreement with some observational evidence for the solar neighbourhood. An exponential cut-off in the low-mass range is also favoured by recent determinations of the local IMF down to the brown dwarf regime (Chabrier 2001, 2002, see below).

This functional form of the IMF was originally introduced by Larson (1986) with the suggestion that the characteristic mass scale M_{L1} may be larger for higher temperatures of the parent gas, as expected for the Jeans mass scale. This would imply a top-heavy IMF in the early galactic phases, at high redshifts and/or in low-metallicity environments. A suitable variation of the typical mass scale M_{L1} could reproduce the systematic variations of M/L ratios in elliptical galaxies (Chiosi et al. 1998) and explain the chemical enrichment of the intracluster medium (Chiosi 2000; Finoguenov, Burkert & Böhringer 2003; Moretti, Portinari & Chiosi 2003) or be responsible for the possible presence of dark massive objects in the Galactic halo (Chabrier 1999).[2]

In the present study, however, we do not consider variations in the IMF with time or metallicity, and within each chemo-photometric model we assume the IMF to be constant.

(v) A modified Larson IMF:

$$\Phi(M) = C_{L2}\, M^{-1.7} \exp\left(-\frac{M_{L2}}{M}\right)$$

$C_{L2} = 0.4337 \quad M_{L2} = 0.425.$

This IMF maintains the same functional form as the original Larson (1998) IMF, but with a steeper slope at high masses in better agreement with local determinations (Scalo 1986; Kroupa 2001). The mass scale M_{L2} is chosen so as to maintain the same peak mass $M_\mathrm{p} = M_{L2}/1.7 = 0.25\,M_\odot$ as in the previous case.

(vi) The IMF suggested by Chabrier (2001, his case IMF3):

$$\Phi(M) = C_\mathrm{C} M^{-2.3} \exp\left[-\left(\frac{M_\mathrm{C}}{M}\right)^{1/4}\right]$$

$C_\mathrm{C} = 40.33 \quad M_\mathrm{C} = 716.4$

over the mass range [0.01–100] $M_\odot$. Chabrier (2001) adopts this functional form, a power law with an exponential cut-off, after Larson (1986) and tunes its parameters to fit the local field IMF in the low-mass range ($M < 1\ M_\odot$), showing also that this form of the IMF is valid down to the brown dwarf regime (Chabrier 2002). In the range of massive stars the steep Scalo/Kroupa slope is recovered.

4 THE SINGLE STELLAR POPULATIONS

A single stellar population (SSP) is a coeval, chemically homogeneous assembly of stars with masses distributed according to the IMF; the integrated spectrum and luminosity $L_\mathrm{SSP}(\tau, Z)$ of an SSP of age τ and metallicity Z can be computed on the basis of stellar isochrones, combined with a spectral library. SSPs are the 'building blocks' of spectrophotometric models of more complex systems, such as galaxies: by convolving SSPs with the SFH $\Psi(t)$ and the metal enrichment history $Z(t)$ provided by chemical models, the corresponding global luminosity in any given passband can be calculated as

$$L = \int_0^T \Psi(t) L_\mathrm{SSP}[T - t,\, Z(T - t)]\, \mathrm{d}t, \qquad (2)$$

where T is the present age of the galaxy.

For the purpose of this paper, we computed SSPs for the IMFs discussed in Section 3, and for metallicities $Z = 10^{-4}, 4 \times 10^{-4}, 0.001$, 0.004, 0.008, 0.019 (=$Z_\odot$), 0.04, 0.07, 0.1. Our SSPs are based on the latest Padua isochrones (Girardi et al. 2000, 2002; Salasnich et al. 2000; http://pleiadi.pd.astro.it), recently extended to $Z = 0.1$ by L. Girardi (private communication). These isochrones are constructed from stellar tracks with updated opacities, equation of state

[2] Note that the Macho-inspired halo IMF suggested by Chabrier (1999) and mentioned here, peaking at 1.7 $M_\odot$, differs from the IMF derived by Chabrier (2001, 2002) for the solar vicinity, peaking around 0.1 $M_\odot$ and used below in this paper.

Table 1. Solar magnitudes in the main Johnson–Cousins–Glass bands as predicted by the stellar libraries in use.

	Girardi/Castelli	Lejeune
Bol	4.720	4.720
U	5.666	5.576
B	5.448	5.446
V	4.788	4.807
R	4.413	4.433
I	4.065	4.080
J	3.640	3.653
H	3.295	3.307
K	3.263	3.252

and neutrino cooling, and with a moderate amount of convective overshoot (see the above-mentioned papers for all details). In this work we consider only isochrones with solar-scaled metallicity; α-enhanced compositions may be found for stars at low metallicities and/or in the inner disc regions, where the SFH is more rapid (see Section 6). Recently, stellar tracks and isochrones with α-enhanced composition have become available for $Z \geqslant 0.008$ (Salasnich et al. 2000); for lower metallicities, suitable conversion formulae from the α-enhanced to the solar-scaled case can be applied (Salaris, Chieffi & Straniero 1993). We will consider the role of α-enhanced compositions in future models.

For the sake of the present study, most notable in these isochrones is that the AGB phase includes up-to-date prescriptions for the thermally pulsing (TP) regime (Girardi & Bertelli 1998); the contribution of AGB stars is very important for the evolution of the near-infrared (NIR) flux and of visual-NIR colours (Girardi & Bertelli 1998; Mouhcine & Lançon 2002; Schulz et al. 2002), and is also potentially interesting for the red bands considered in the present paper. The effect of including full semi-analytical models of the TP-AGB phase in the isochrones and SSPs will be discussed in Section 5.2, by considering the isochrones by Marigo & Girardi (2001) as an alternative set. We stress that a consistent inclusion of all post-main-sequence phases of stellar evolution in the computation of isochrones and SSPs is crucial for a correct estimate of the integrated luminosity and of M/L ratios (Buzzoni 1999, 2002).

The transformation from theoretical quantities ($L_{\rm bol}$, $T_{\rm eff}$, g) into magnitudes and colours is performed through the spectral library compiled by Girardi et al. (2002), a suitable extension of Kurucz' ATLAS9 library (Castelli, Gratton & Kurucz 1997). From the same library we derive for the solar model of the Padua tracks ($\log T_{\rm eff} = 3.762$, $\log\ g = 4.432$, L. Girardi, private communication) the solar absolute magnitudes listed in Table 1, first column. To express integrated luminosities of photometric models in solar units, in fact we consider it more consistent to refer to the theoretical solar magnitudes derived from the same spectral library, rather than to the observed ones or to the magnitudes given by more detailed solar spectrum models; differences are never the less well below 0.1 mag in the bands of interest. Uncertainties related to the use of different libraries are briefly discussed in Section 5.3, by means of SSPs calculated using the Lejeune library.

For further details on the calculation of SSPs, the reader is referred to Bressan, Chiosi & Fagotto (1994) and Tantalo et al. (1996). For consistency with previous work, in the SSPs the adopted solar bolometric magnitude and the definition of the bolometric corrections are slightly different from those in Girardi et al. (2002). However, when allowance is made for the different definition of the zero-points, the integrated luminosities are identical in the two cases and the predicted M/L ratios are unaffected, as expected.

5 A DISCUSSION OF SIMPLE MODELS

For a preliminary study of the effect of different IMFs on the M/L ratio, we first resort to very simple models, adopting an exponentially decaying star formation rate

$$\Psi(t) \propto {\rm e}^{-t/\tau_{\rm SF}},$$

where different time-scales $\tau_{\rm SF}$ correspond to different values of the b parameter (equation 1). The age of the model discs is assumed to be $T = 10$ Gyr, as estimated for the bulk of the stellar population in the disc of the Milky Way (Carraro 2000). Exponentially decaying SFRs with varying time-scales have often been used as effective prescriptions to reproduce the Hubble sequence in spectrophotometric models (e.g. Larson & Tinsley 1978; Bruzual 1983; Guiderdoni & Rocca-Volmerange 1987; Bruzual & Charlot 1993; KTC94; Möller, Fritze-v. Alvensleben & Frick 1997; Bell & de Jong 2000). Our preliminary 'exponential' models do not include chemical evolution, but we can learn about the role of metallicity by adopting SSPs of different metallicities in equation (2). These simple models are also useful for assessing uncertainties related to the detailed prescriptions for the TP-AGB phase and to the adopted stellar library (Sections 5.2 and 5.3).

Fig. 4 shows the stellar (i.e. stars+remnants) M/L ratio in the I band for our exponential models as a function of the corresponding b parameter; different panels correspond to models with different IMFs. Metallicities between ∼half solar and solar are considered representative of the bulk of stars in galactic discs. The shaded area indicates the range of observed $M/L_I = 0.7$–1 we want to reach with our Sbc–Sc disc models ($b = 0.8$–1, see Section 2).

It is immediately apparent how a Salpeter IMF yields a M/L ratio much higher than desired. The local Kroupa IMF still has a slightly high $M/L_I \gtrsim 1$, while all the other 'bottom-light' IMFs generally reach $M/L_I \leqslant 1$ for the models corresponding to Sbc/Sc spirals. This overview promotes the development of more refined models for a detailed prediction of M/L ratios with bottom-light IMFs (Section 6).

Fig. 5 shows for two examples, the Salpeter and the Kennicutt IMFs, the predicted M/L ratios of the global stellar population (i.e. stars and remnants, thick lines) compared with the M/L ratio of the sole population of living stars (thin lines). Neglecting the mass of stellar remnants (white dwarfs, neutron stars and black holes) induces an underestimate of the M/L ratios typically of 10 per cent, which can increase by up to 30 per cent, depending on the IMF and SFH (cf. models with low-b parameter and Kennicutt IMF). This illustrates the importance of calculating self-consistently the contribution of stellar remnants when discussing the M/L ratio of the stellar/baryonic component of galaxies.

5.1 Dependence of the M/L ratio on Hubble type

It is interesting to consider the variation of stellar M/L ratios with Hubble type, here parametrized by the b parameter indicative of the different star formation histories. Fig. 6 shows the M/L ratio as a function of b, *normalized* to the value corresponding to $b = 1$. The scale on the right axis indicates the corresponding shift in magnitude. The plot is for different IMFs and for solar metallicity; results for *relative* M/L ratios do not change considering the case $Z = 0.008$ instead. In the I band (top panel in Fig. 6) with respect to

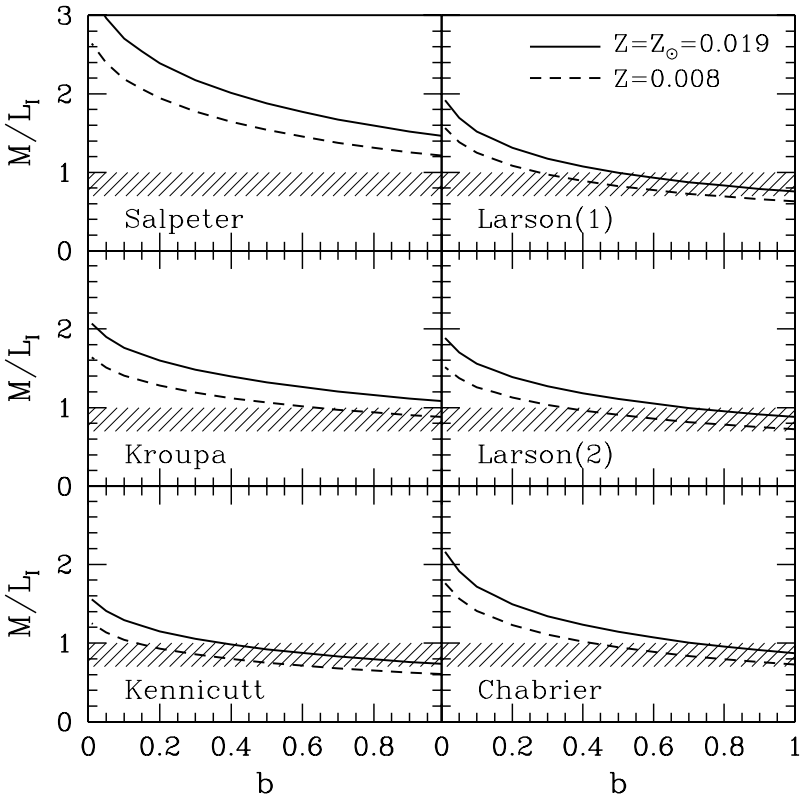

Figure 4. M/L ratio in the I band for simple exponential models with varying b parameter; different panels correspond to models with different IMFs, as indicated. The shaded area marks the range $M/L_I = 0.7$–1 favoured by observations of Sbc–Sc discs ($b = 0.8$–1). This figure is available in colour in the on-line version of the journal on *Synergy*.

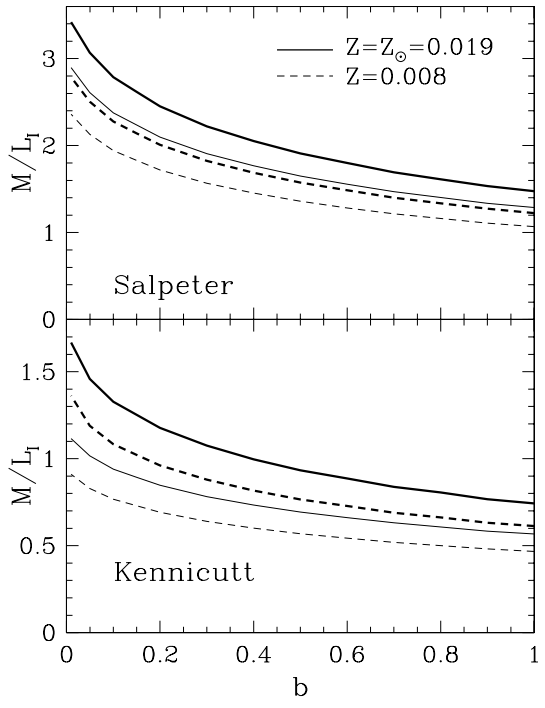

Figure 5. I-band M/L ratio for the global stellar population (stars+remnants, thick lines) compared with that of the sole living stars (thin lines). The mass of remnants typically contributes for a 10 per cent, but it can reach 30 per cent for bottom-light IMFs, such as the Kennicutt IMF and SFHs skewed to old populations (low-b parameters). This figure is available in colour in the on-line version of the journal on *Synergy*.

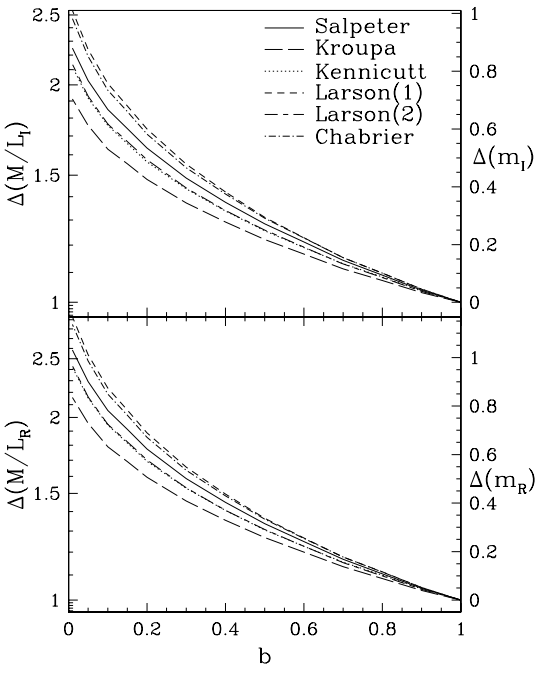

Figure 6. Relative M/L ratio normalized to the value corresponding to $b = 1$ models. Top panel, I band; bottom panel, R band. Results are plotted for different IMFs as indicated, for solar metallicity. This figure is available in colour in the on-line version of the journal on *Synergy*.

Sbc–Sc spirals we predict the M/L ratio to increase by a factor of 1.3–1.5 for Sb spirals ($b \sim 0.35$) and of 1.7–2.2 for Sa–Sab spirals ($b \sim 0.1$). This corresponds to a systematic magnitude offset of 0.3–0.4 mag and of 0.6–0.8 mag for Sb and for Sa–Sab spirals, respectively, as a result of the difference in characteristic SFH. These offsets are somewhat reduced when bulges are included in the computation of the total M/L ratios of galaxies (Section 8.1), but they remain significant. The offsets we predict are larger than the empirical ones found by Giovanelli et al. (1997a): 0.1 mag for Sb spirals and 0.32 mag for earlier types. However, the extent of systematic offsets in the TF relation is still a matter of debate: for instance, larger offsets in the nearby R band are found by Kannappan et al. (2002). Their offset of 0.76 mag for Sa galaxies is in good agreement with our predictions in the R band at $b \sim 0.1$ (Fig. 6, lower panel).

5.2 The treatment of the AGB phase

For SSPs of intermediate age, the luminosity (in particular the bolometric and NIR) is dominated by the contribution of stars in the AGB phase. Hence careful modelling of these phases of stellar evolution is very important when determining M/L ratios, especially in the NIR.

As underlined in Section 4, our SSPs are based on isochrones (Girardi et al. 2002), which explicitly include the TP-AGB phase with a synthetic algorithm based on the core growth, the core mass–luminosity relation and the initial–final core mass relation (Girardi & Bertelli 1998). Recently, Marigo & Girardi (2001) discussed self-consistency between chemical and photometric evolution in galactic models. They refined the calculation of the 'stellar fuel' (amount of hydrogen or helium consumed by nuclear burning) adding the contribution of the chemical yields dredged up and lost by the stars, to the classic fuel estimate based only on the initial–final core mass relation. According to the fuel consumption theorem (Renzini & Buzzoni 1986), this additional fuel corresponds to additional emitted luminosity (mostly in the NIR for AGB stars). Marigo & Girardi also provide isochrones including detailed semi-analytical models for the TP-AGB phase, improving upon the simple synthetic algorithm adopted by Girardi et al.

In this section, we check the effect of a different modelling of the TP-AGB phase on the predicted M/L ratios in galactic discs. We calculated a set of SSPs based on the isochrones by Marigo & Girardi (M-SSPs) to be compared with our reference SSPs based on the isochrones by Girardi et al. (G-SSPs). Fig. 7 compares the luminosity evolution of the G-SSPs (thick lines) with that of the M-SSPs (thin lines) for the three metallicities available for the M-SSPs; we adopt a total SSP mass of 1 $M_\odot$ and the Salpeter IMF for the sake of illustration. With the M-SSPs, although the onset of the AGB contribution is more gradual (with a smoother phase transition due to the overluminosity effect, see Girardi & Bertelli 1998), the overall luminosity produced in the course of evolution is larger, as expected from the larger 'fuel' actually consumed. The effect is generally negligible in the I band (and in all other optical bands) with the exception of very low metallicities, but it is highly significant in the NIR; in the K band, the M-SSPs can be up to 0.6 mag brighter.

Fig. 8 compares the M/L ratios of our simple exponential models for discs, as predicted with the G-SSPs and with the M-SSPs. In the I band the difference is minor, and negligible for the relevant metallicities $Z \geqslant 0.008$, while in the K band it becomes significant (up to 20–30 per cent). The Salpeter IMF is adopted for the sake of illustration, but the situation is similar for all the other IMFs.

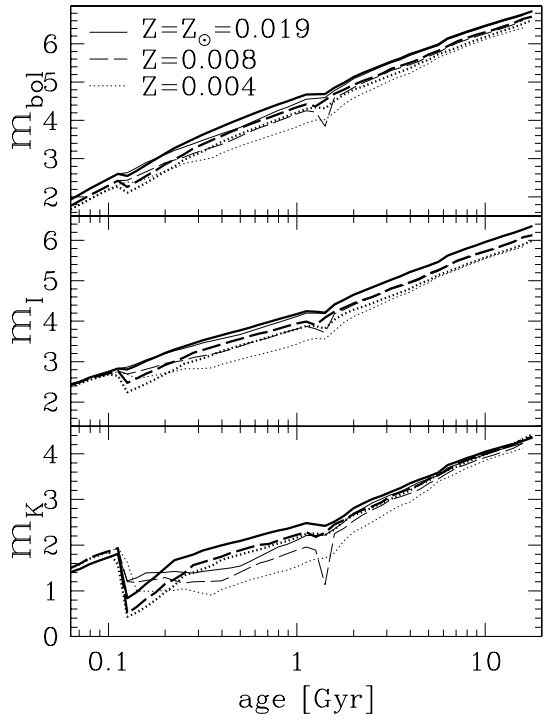

Figure 7. Comparison between the G-SSPs and the M-SSPs (thick and thin lines, respectively) in bolometric, I and K magnitude. Detailed modelling of the TP-AGB phase (M-SSPs) leads to a larger overall luminosity contributed by AGB stars, mostly in the K and NIR bands. For the M-SSPs with $Z = 0.008$, note the occurrence of a 'red spike' around 1.5 Gyr, a feature discussed by Girardi & Bertelli (1998). This feature is very short lived and does not influence the bulk of emitted light integrated over time. This figure is available in colour in the on-line version of the journal on *Synergy*.

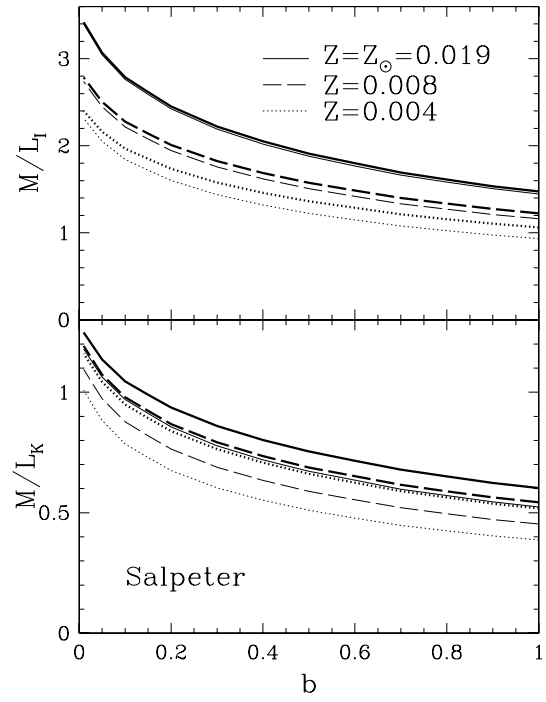

Figure 8. M/L ratios for our exponential disc models, as obtained with the G-SSPs and the M-SSPs (thick and thin lines, respectively). This figure is available in colour in the on-line version of the journal on *Synergy*.

In summary, the effect of detailed TP-AGB modelling is negligible in the *I* band (and in optical bands in general), making, from this point of view, the *I*-band luminosity superior to NIR luminosities for mass estimates.

Stellar and photometric evolution in the TP-AGB phase can be further altered by dusty circumstellar envelopes (Bressan, Granato & Silva 1998; Mouhcine 2002; Piovan, Tantalo & Chiosi 2003) or different opacities and mass-loss rates in the carbon star phase (Marigo 2002; Marigo, Girardi & Chiosi 2003). Again, the effects are seen mostly in the NIR colours but they should be negligible for the integrated *I*-band luminosity, where the contribution of AGB stars is not so dominant. We conclude that estimates of M/L ratios in the *I* band are robust with respect to uncertainties in the modelling of the TP-AGB phase.

5.3 An alternative spectral library

An alternative spectral library has been provided recently by Lejeune, Cuisinier & Buser (1997, 1998) and has been widely used in population synthesis studies (Boissier & Prantzos 1999; Liu, Charlot & Graham 2000; Schulz et al. 2002). This is also an extension of the synthetic Kurucz' ATLAS9 library, but with additional empirical corrections to reproduce the observed colour–temperature relations of individual stars. However, Girardi et al. (2002) argue against a posteriori calibrations of theoretical libraries, while Westera et al. (2002) find that it is not possible to attain a semi-empirical library that could reproduce both empirical colour–temperature relations and, when combined with current isochrones, the observed colour–magnitude diagrams of star clusters.

Thus, the present status of semi-empirical libraries is not yet fully satisfactory; it is still useful, however, to discuss these alternative libraries in connection with uncertainties in integrated magnitudes due to the spectral input. To this end we calculated an alternative set of SSPs based on the same isochrones as the G-SSPs (see Section 4) but adopting the semi-empirical library by Lejeune et al. (1997, 1998). We indicate this alternative set as L-SSPs; the corresponding solar magnitudes, derived for the solar model linked to the Lejeune library, are listed in Table 1. The difference between the G-SSPs and the L-SSPs is prominent in the $V-I$ colour (Fig. 9) making the L-SSPs brighter in the *I* band by up to 0.1 mag at intermediate and old ages (since the absolute *V* magnitude is no different between the two sets). This is purely an effect of the spectral library, and makes

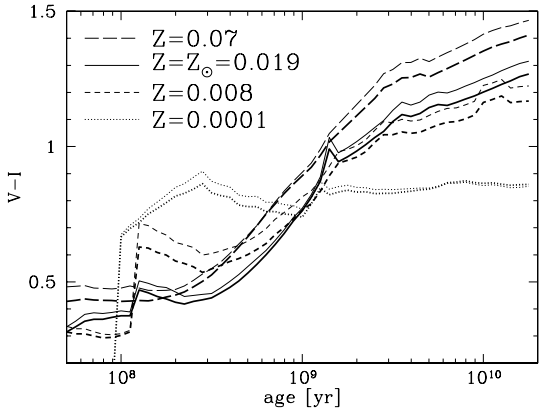

Figure 9. Comparison between the G-SSPs and the L-SSPs (thick and thin lines, respectively) in $V-I$. The Lejeune library predicts redder $V-I$ colours, hence more light in the *I* band. The Kroupa IMF is adopted here for the sake of example, however, the age evolution of $V-I$ is insensitive to the IMF. This figure is available in colour in the on-line version of the journal on *Synergy*.

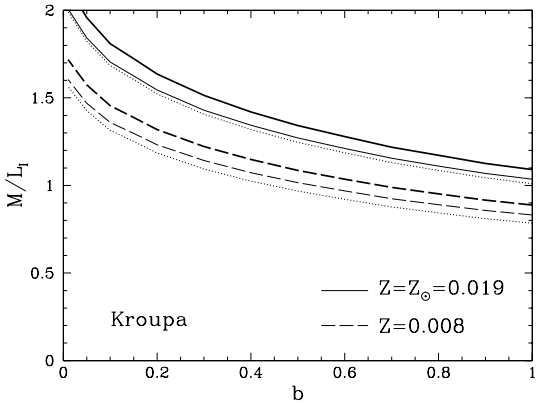

Figure 10. M/L ratios for our exponential disc models obtained with the L-SSPs (thin lines) as compared with the 'standard' G-SSPs (thick lines). Dotted lines for the LM-SSPs. The Kroupa IMF is adopted here for the sake of example. This figure is available in colour in the on-line version of the journal on *Synergy*.

our model M/L ratios in the *I* band lower by a 5–10 per cent, when the L-SSPs are adopted (Fig. 10).

Finally, we checked whether a more refined treatment of the AGB phase would have a sizeable effect on the predicted M/L ratios with the Lejeune library, where red giants are more luminous in the *I* band. The effect of a detailed inclusion of the TP-AGB phase, from the isochrones by Marigo & Girardi (2001), was found to be small in the *I* band when the Girardi/Castelli library was adopted (Section 5.2 and Fig. 8). If the Marigo & Girardi isochrones are combined with the Lejeune library (set LM-SSPs), again the effects on the *I*-band M/L ratio is small with respect to the results from the L-SSPs (Fig. 10). In conclusion, with present models the *I*-band luminosity is more affected by the adopted spectral library than by the detailed modelling of the AGB phase.

Since the situation with semi-empirical libraries is still somewhat dichotomous (Westera et al. 2002), in the remainder of the paper we will adopt as our standard set the G-SSPs based on the theoretical spectral library by Girardi/Castelli. However, from the discussion above and from Figs 8 and 10, it is apparent that current alternative spectral libraries (and, marginally, a more refined modelling of the AGB phase) tend to increase the predicted *I* luminosity. Therefore, our predictions for M/L ratios in the *I* band will be conservatively high, though not by a large amount (at most 10 per cent).

6 CHEMO-PHOTOMETRIC MODELS

More realistic photometric models for galactic discs should include star formation histories and corresponding chemical evolution consistently. From chemical evolution studies of the solar neighbourhood, especially from the G-dwarf problem (Lynden-Bell 1975; Tinsley 1980; Pagel 1997 and references therein), and from dynamical models of the formation of galactic discs (Larson 1976; Sommer-Larsen 1991; Burkert, Truran & Hensler 1992; Sommer-Larsen, Götz & Portinari 2003) it is well known that galactic discs form gradually by slow accretion ('infall') of primordial or low-metallicity gas. Correspondingly, the SFR is expected first to increase, following increasing available gas, reach a maximum and later decrease due to gas consumption (Fig. 11).

Moreover, the metallicity and colour gradients observed in the Galactic disc and external disc galaxies, indicate that the star formation and chemical enrichment history typically proceeds at a different (slower) pace at increasing galactocentric radius

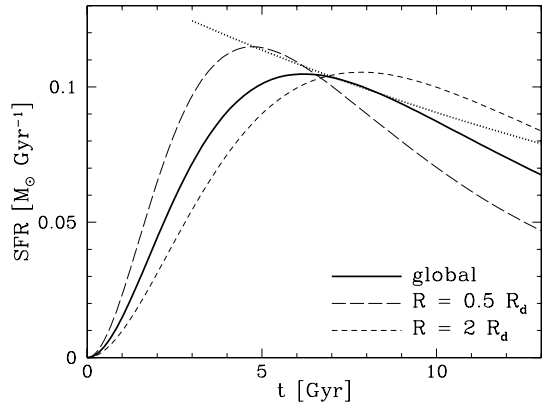

Figure 11. Star formation history for the disc of model SALP-A (between $R = 0.5 - 3h_B$, see Section 6.3). For comparison, the dotted line shows the SFH of a simple exponential model with the same $b = 0.79$ and age 10 Gyr. The long-dashed and short-dashed lines illustrate the different pace of the SFH at different galactocentric distances, characteristic of inside–out models. For the sake of comparing the respective shape, all the SFR curves are normalized to the same integrated SFH of 1 $M_\odot$. This figure is available in colour in the on-line version of the journal on *Synergy*.

(inside–out scenario, Matteucci & François 1989; Chiappini, Matteucci & Gratton 1997; Fig. 11; but see also Sommer-Larsen et al. 2003). A realistic SFH for a disc galaxy is therefore more complex than the monotonic, exponential form adopted in the simple models of Section 5.

As a basis for our photometric models, we develop a series of chemical evolution models with infall, and with a multizone radial structure so that gradients of metallicity and SFH can be reproduced. The reader not keen on the details of model construction and calibration on to the observable constraints, nor on the detailed discussion of the sets of models with each specific IMF, can directly find an overview of the results in Section 7.5.

We make use of the chemical evolution code by Portinari, Chiosi & Bressan (1998); Portinari & Chiosi (1999). The disc is assumed to have an exponential surface density profile:

$$\sigma(R) = \sigma_{\rm d}\, {\rm e}^{-(R-R_{\rm d})/R_{\rm d}}, \tag{3}$$

where $\sigma(R)$ is the present-day total surface density distribution, $R_{\rm d}$ is the scalelength of the mass distribution and $\sigma_{\rm d}$ is the surface density at a distance $R = R_{\rm d}$ from the centre. The disc is typically divided into 26 zones, 0.2 $R_{\rm d}$ wide, between $R = 0$ and 5 $R_{\rm d}$.

In each zone infall is assumed to occur, as customary, at an exponentially declining rate

$$\frac{{\rm d}\sigma}{{\rm d}t} \propto \exp\left(-\frac{t}{\tau_{\rm inf}}\right),$$

where the infall time-scale may vary with radius, $\tau_{\rm inf} = \tau_{\rm inf}(R)$, typically increasing outward in the inside–out scenario. A similar behaviour of the infall process, exponentially declining rates with time-scales increasing outward, is also found in some recent cosmological/hydro-dynamical simulations of the formation of galactic discs (Sommer-Larsen et al. 2003).

We assume $T = 13$ Gyr for the age of the models, as suggested by the Λ-cold dark matter simulations of Sommer-Larsen et al., where the SF activity associated with the main galaxy typically starts at a redshift of 4–5. This is larger than the age of 10 Gyr assumed in our exponential models in Section 5, but one should bear in mind that the latter represents the age of the *bulk* of local disc stars. In an infall scheme, the formation of the disc is described since the very early stages of gas accumulation; SF develops gradually, reaches its maximum after a few Gyrs and then declines, so that the bulk of stars form in fact during the last ∼10 Gyr (Fig. 11).

As to the SF law, we adopt the form suggested by Dopita & Ryder (1994):

$$\frac{{\rm d}\sigma_*}{{\rm d}t} \propto \sigma^{1/3}\sigma_{\rm g}^{5/3}$$

depending both on the gas surface density $\sigma_{\rm g}$ and on the total surface density σ; σ_* is the surface density of stars. This is a Schmidt-like law (Schmidt 1959) with efficiency decreasing at increasing radius through the dependence on $\sigma(R)$, as supported by both theoretical and empirical arguments (Dopita & Ryder 1994). The resulting SFHs are necessarily faster in the inner regions and slower in the outer ones where the surface density is lower; this SF law results in metallicity gradients comparable to the observed ones (Portinari & Chiosi 1999). With a convenient normalization (see Portinari & Chiosi 1999 for details) we express this law

$$\frac{\rm d}{{\rm d}t}\sigma_*(R,t) = \nu\frac{\sigma^{1/3}(R,t)\,\sigma_{\rm g}^{5/3}(R,t)}{\sigma(R_{\rm d},T)},$$

where ν is the star formation efficiency in units of $[t^{-1}]$. The code performs detailed calculations of the delayed gas and metal restitution from stars of various lifetimes, including supernovae (SNe) of type Ia, and of the evolution of the abundances of the main chemical elements; we refer to Portinari et al. (1998) for all details on the chemical model and to Portinari & Chiosi (1999) for the implementation of the SF law and of the multizone scheme. With respect to the above-mentioned papers, the present models are updated in the input yields of low- and intermediate-mass stars (Marigo 2001), which are consistent with the TP-AGB calculations included in the M-SSPs (Section 5.2).

Our models are a two-parameter family, with parameters: $\tau_{\rm inf}$, infall time-scale (in Gyr, not to be confused with the SF time-scale $\tau_{\rm SF}$ of the simple models in Section 5) and ν, SF efficiency (in ${\rm Gyr}^{-1}$).

This pair of parameters will be tuned, for each selected IMF, so as to reproduce two main constraints discussed below, the first selecting the relevant SFHs, and the second setting the level of metal enrichment and the gas fraction.

6.1 Constraints on the SFH

From the SFH of each model we can define its b parameter:

$$b = \frac{\psi(T)}{\langle\psi\rangle} \qquad \langle\psi\rangle = \frac{1}{T}\int_0^T \psi(t)\,{\rm d}t, \tag{4}$$

where $\Psi(t)$ is the instantaneous global SFR. We select the models with $b = 0.8$–1 as representative of Sbc–Sc discs, as discussed in Section 2; the corresponding typical intrinsic $B - V$ colour is $(B - V)_0 \sim 0.55$ (Roberts & Haynes 1994).

6.2 Constraints on chemical evolution

A second constraint is the 'typical chemical properties' of an Sbc–Sc disc. Non-barred spirals exhibit an oxygen gradient in the gas component that seems to be roughly independent of Hubble type, once radii are expressed in units of scalelength (in the B band) rather than in physical distance units such as kiloparsecs. The typical average value is

$$\frac{\rm d}{{\rm d}R}\left[\frac{\rm O}{\rm H}\right] = -0.2\,{\rm dex}\; h_B^{-1}$$

with values ranging between −0.1 and −0.3 dex h_B^{-1} (Garnett et al. 1997; van Zee et al. 1998; Prantzos & Boissier 2000). Oxygen can be taken as a tracer of the global metal content, as it is the most abundant metal and it generally contributes roughly half of the overall metallicity. In the following the term 'metallicity' will often be used in place of 'oxygen abundance', for the sake of simplicity.

The typical disc gas metallicity, usually defined as the central value extrapolated from the observed gradient or, more directly, the metallicity at a galactocentric distance $R = h_B$, shows a marked dependence on mass. The samples by Garnett et al. and van Zee et al., and those by KTC94 and Roberts & Haynes (1994) considered above in the paper, mostly consist of galaxies with magnitude around $M_B = -21$ (when all rescaled to the same $H_0 = 50$). Therefore, we will discuss mainly bright galaxies with sizes comparable to the Milky Way, while we do not investigate in this paper mass-dependent behaviours. The dependence of the typical metallicity on Hubble type seems to be a secondary relation, mostly a consequence of the mass–metallicity relation through the Hubble type–mass relation; there is in fact a tendency for earlier Hubble types to be more massive, though with a large overlap in mass between types.

For Milky Way sized galaxies, from the samples of Garnett et al. and van Zee et al. we derive a typical metallicity of Sbc–Sc discs of

$$12 + \log\left(\frac{\mathrm{O}}{\mathrm{H}}\right) = 9.1\,\mathrm{dex} \qquad \text{at } R = h_B.$$

We will use this typical metallicity and metallicity gradient to constrain our chemical evolution models.

Another significant constraint for chemical models is the gas fraction, that is the final ratio between the gas mass and the total baryonic mass (Tinsley 1980; Pagel 1997)

$$f_{\mathrm{gas}} = \frac{M_{\mathrm{gas}}}{M_{\mathrm{gas}} + M_*}$$

in obvious notation. Hence we need an estimate of the typical gas fraction in Sbc–Sc discs. This in turn requires an estimate of the stellar mass M_*, which can only be obtained from the observed luminosity and an assumed stellar M/L ratio (one cannot use dynamical mass estimates because of the unknown contribution of dark matter). However, since the M/L ratio is supposed to be a prediction of our models we should make no a priori assumptions concerning it, and in place of the usual gas mass fraction we consider as a constraint the gas-to-luminosity fraction

$$f_{L,\mathrm{gas}} = \frac{M_{\mathrm{gas}}}{L_B}.$$

This quantity, besides being independent of any assumed M/L ratio, has the additional advantage of being independent of distance and hence of H_0. As the mass of gas (H I + H_2) is derived from the observed flux in the 21 cm line and in the CO lines, which have the same dependence on the assumed distance as L_B, their ratio is distance independent.

Roberts & Haynes (1994) give for Sbc–Sc galaxies a typical value of

$$\frac{M(\mathrm{H\,I})}{L_B} = 0.30^{+0.18}_{-0.12}\frac{\mathrm{M}_\odot}{\mathrm{L}_\odot}.$$

Comparable values can be derived from the samples of de Mello, Maia & Wiklind (2002a) and de Mello, Wiklind & Maia (2002b), and just slightly lower ones from that of KTC94. The masses of neutral hydrogen quoted here are the global masses for the whole H I disc. For the sake of chemical evolution, however, the significant constraint is the gas fraction within the area of active star formation, i.e. limited to within the optical radius. Some corrections to the above quantities should be applied to account for the fact that the H I disc generally extends further than the optical disc. Considering the sample of spirals of KTC94, it is possible to correct from the total gas mass to the gas mass within the optical radius, using the 'Roberts times' listed in their table 5. We obtain typical corrections of 0.6 for field spirals and 0.8 for cluster spirals, the outer gaseous discs of which are presumably stripped because of the dense environment, and hence less extended beyond the optical disc. Since the large sample of Roberts & Haynes, from the RC3 catalogue, contains both field and cluster spirals, we apply an average correction of 0.7 to derive the gas masses within R_{25}. This also agrees with the corrections of 0.66–0.72 derived by Sommer-Larsen (1996).

As to the molecular component, Young & Knezek (1989) give for Sbc–Sc galaxies

$$\frac{M(\mathrm{H_2})}{L_B} = 0.16^{+0.02}_{-0.02}\frac{\mathrm{M}_\odot}{\mathrm{L}_\odot}.$$

We find similar values in the sample of KTC94 and somewhat lower values (∼0.1) in the sample of de Mello et al.[3] Adding the two components, we derive

$$\frac{M(\mathrm{H\,I} + \mathrm{H_2})}{L_B} = 0.3\text{–}0.37$$

and including the standard factor of 1.4 for the contribution of other elements (mostly helium) to the total gas mass, we finally derive

$$f_{L,\mathrm{gas}} \sim 0.42\text{–}0.52$$

as a typical gas-to-luminosity fraction for Sbc–Sc galaxies.

This value is broadly compatible with the analogous quantity in our Milky Way Disc. The masses of neutral and molecular hydrogen in our galaxy, within the optical radius of the disc, are $M(\mathrm{H\,I}) = 4.3 \times 10^9$ and $M(\mathrm{H_2}) = 1.3\text{–}1.7 \times 10^9$ $\mathrm{M}_\odot$ (Dame 1993; Binney & Merrifield 1998). We can estimate the total B-band luminosity of the Milky Way as follows: the K-band luminosities of the disc and bulge are, respectively, $L_{K,\mathcal{D}} = 4.9 \times 10^{10}\,\mathrm{L}_\odot$ and $L_{K,\mathcal{B}} = 1.1 \times 10^{10}\,\mathrm{L}_\odot$ (Kent, Dame & Fazio 1991; Binney & Merrifield 1998); considering $(B - K) = 3.51$ as typical for an Sbc–Sc spiral (de Jong 1996b), for our Milky Way we obtain a global $L_B \sim 1.8 \times 10^{10}$ $\mathrm{L}_\odot$. Including the standard 1.4 factor for the helium correction to the gas mass, we derive for the Milky Way $f_{L,\mathrm{gas}} \sim 0.45$.

Finally, as we model the SFH and the chemical evolution of galactic discs, we should adopt for the gas-to-luminosity fraction the luminosity of the disc only. So, we must correct for the contribution of bulges to the total B luminosity. For Sbc–Sc galaxies, the average bulge contribution is estimated to be $L_{B,\mathcal{B}}/L_B \sim$ 10–20 per cent (Simien & de Vaucouleurs 1986; de Jong 1996a), which implies

$$f_{L,\mathrm{gas},\mathcal{D}} \sim 0.45\text{–}0.55.$$

We therefore adopt 0.5 ± 0.05 as our constraint for the chemical enrichment level. However, this 'gas fraction' constraint is much less firm than the observed metallicities, for it has been derived by assembling a number of independent observational studies and applying various corrections.

[3] Recently, Boselli, Lequeux & Gavazzi (2002), applying a calibrated conversion factor χ between CO emission and H_2 mass depending on metallicity, ultraviolet (UV) field and galaxy luminosity, derived a much lower typical $M(\mathrm{H_2})/M(\mathrm{H\,I}) \sim 0.15$. They suggest that previous studies, adopting a constant conversion factor, overestimated the molecular mass in bright galaxies, while underestimating it in faint galaxies, by a factor of 2–3. If so, our estimates of the gas-to-luminosity fractions above are upper limits, and the bulk of the gas would lie in the H I component.

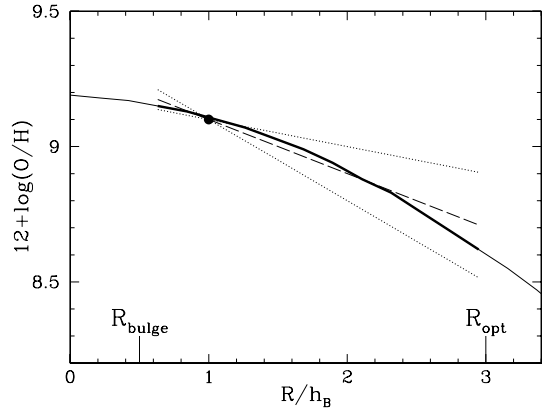

Figure 12. Metallicity gradient in the present-day gas phase for model SALP-A, with radius in units of B-band scalelength h_B. The significant 'disc region' is marked as a thick line. The solid dot marks the observational calibration point 9.1 for metallicity at $R = h_B$. The dashed line is the observed average gradient -0.2 dex/h_B, the dotted lines mark the limits of the broad range of observed gradients, between -0.1 and -0.3 dex/h_B. This figure is available in colour in the on-line version of the journal on *Synergy*.

6.3 Calibration of the models

For each of the six considered IMFs, we develop a grid of models with different time-scales $\tau_{\rm inf}$. For each model, the SF efficiency ν is fixed so that the final gas metallicity is $12 + \log(\mathrm{O/H}) \sim 9.1$ dex at $T = 13$ Gyr and at a radius $R = h_B$ (see the discussion in Section 6.2 and Fig. 12). Among these models with specific (ν, $\tau_{\rm inf}$) combinations, we select those where the global SFHs correspond to $b = 0.8$–1, that is to Sbc–Sc discs. This corresponds to selecting tendentially models with long infall time-scales, as larger $\tau_{\rm inf}$ s induce longer SFHs and hence larger b values. The parameters and characteristics of the selected models are listed in Table 2.

The adopted SF law often generates metallicity gradients in broad agreement with the observed ones, for it results in an inside–out SFH even when $\tau_{\rm inf}$ is constant with radius. Only when necessary do we include a radial increase of the infall time-scale $\tau_{\rm inf}(R)$ reinforcing the inside–out behaviour (see model SALP-C in Fig. 13).

To illustrate our procedure, here we describe in detail the calibration of the models with the Salpeter IMF. The comparison to the results for the other 'bottom-light' IMFs will be discussed in the next section.

Model SALP-A adopts $\tau_{\rm inf} = 5$ Gyr, and the SF efficiency is fixed to be $\nu = 0.47$ Gyr^{-1} to obtain an oxygen abundance of 9.1 dex at the reference radius $R = h_B$ (Fig. 12). We calculate the disc photometry by applying equation (2) to each individual annulus with its specific SFH $\Psi(R, t)$ and metal enrichment history $Z(R, t)$, to obtain the surface brightness profiles in Fig. 14. With an underlying exponential mass distribution, the light profile resulting from chemo-photometric models is not perfectly exponential, but close enough that a luminosity scalelength can be defined at least within $\sim$2–3 $R_{\rm d}$ (see also Boissier & Prantzos 1999 for similar results). In model SALP-A, we derive a B-band scalelength $h_B \sim 0.95\ R_{\rm d}$ within the inner $\sim$3 $R_{\rm d}$. Fig. 14 also shows that the redder the band, the shorter the corresponding scalelength is, as expected and as also observed in the Milky Way (Boissier & Prantzos 1999 and references therein).

Computing h_B is necessary to define the limit of the optical disc, which is the region to be compared with actual observations. A typical central (extrapolated) value of the surface brightness of discs is $\mu_{B0} = 21.7$ mag arcsec^{-2} (Freeman 1970), although with a large scatter between 20 and 22 mag arcsec^{-2} (for Hubble types up to Sc, de Jong 1996a); the optical radius R_{25} corresponds to $\mu_B = 25$, or $R_{25} \sim 3$–$4h_B$ from $\mu_B(R) = \mu_{B0} + 1.086R/h_B$. For the following, we define operationally the optical disc as the region within $R_{\rm opt} = 3\ h_B$; we verified that taking 3.5 or $4h_B$ as the limit would not influence the global M/L ratios or gas fractions, since the outskirts of the disc are characterized by a low surface density and brightness, and do not contribute significantly to the global values.

We also exclude from our analysis the innermost $0.5h_B$, where the bulge typically lies in real disc galaxies.

Also the metallicity constraints derived from observations are expressed in terms of the B-band scalelength h_B, rather than the scalelength $R_{\rm d}$ of the underlying mass distribution (equation 3). In Fig. 12 the oxygen abundance profile is plotted as a function of R/h_B, such as for actual observations; the model gradient is well within the typical observed range.

Longer infall time-scales tend to produce shallower metallicity gradients at the present time. With $\tau_{\rm inf} = 10$ Gyr, the gradient is very shallow if $\tau_{\rm inf}$ is constant over the disc; we obtain a gradient of approximately -0.2 dex/h_B only by adopting a radially increasing infall time-scale (model SALP-C, Fig. 13; Table 2).

7 MODEL RESULTS

In this section we present the resulting M/L ratios and chemical properties of our full chemo-photometric models. First, we discuss results for the Salpeter IMF, then for the other, 'bottom-light' IMFs. All models are calibrated to reproduce the observed metallicity distributions and SFHs, as described in Section 6.3; the calibrated parameters and model results are all listed in Table 2.

7.1 Salpeter models

The I-band M/L ratios for the disc models SALP-A-B-C, adopting the Salpeter IMF with the standard mass limits [0.1–100] $\mathrm{M}_\odot$, are shown as solid circles in Fig. 15 as a function of the corresponding b parameter. Also shown as a continuous thin line is the prediction from the simple exponential models of Section 5, with solar metallicity. The full chemo-photometric models confirm quite well the high $M/L_I \sim 1.5$ predicted by the simple models for the Salpeter case.

One should not infer, however, from the agreement with the simple models that photometric computations at constant solar metallicity (such as those in Section 5) are sufficient. In fact, if we calculate the luminosity of the full chemical models SALP-A-B-C using only SSPs with $Z = \mathrm{Z}_\odot$, we obtain higher M/L ratios (open circles in Fig. 15), mainly because of a slightly larger average age of stars in realistic models (with $T = 13$ Gyr) with respect to the simple exponential ones (with $T = 10$ Gyr). In full chemo-photometric models, this is compensated by the fact that an important fraction of the long-lived stars contributing to the I-band luminosity forms at metallicities below solar, lowering the M/L ratio with respect to calculations at fixed $Z = \mathrm{Z}_\odot$ (solid circles versus open circles; see also the M/L ratios at $Z = 0.008$ in Fig. 4). So, the agreement with the simple exponential models with solar metallicity is the complex result of combining a more realistic, radially dependent SFH, with metallicity-dependent photometric calculations.

The crosses in Fig. 15 represent the result of calculating the photometry of models SALP-A-B-C including only SSPs of metallicity $Z \leqslant \mathrm{Z}_\odot$, adopting SSPs of $Z = \mathrm{Z}_\odot$ for larger metallicities. The difference with respect to the reference models is marginal, indicating that super-solar and solar metallicity stars contribute to the

Table 2. List of models with calibrated parameters (columns 3–5) and results (columns 6–10). (1) Model name. (2) Adopted IMF with corresponding mass limits. (3) Infall time-scale $\tau_{\rm inf}$ at $R = h_B$, in Gyr. (4) SF efficiency ν, in Gyr^{-1}. (5) Radial dependence of the infall time-scale. (6) Scalelength of the B-band profile. (7) b parameter of the SFH (equation 4). (8) M/L ratio in the I band for the stellar component (stars+remnants). (9) Intrinsic $(B-V)$ colour of the disc (including the central regions, i.e. between $R = 0$ and $3h_B$). (10) Gas-to-luminosity fraction.

(1) Model	(2) IMF	(3) $\tau_{\rm inf}$	(4) ν	(5) $\tau_{\rm inf}(R)$	(6) $h_B/R_{\rm d}$	(7) b	(8) M_*/L_I	(9) $(B-V)_0$	(10) $M_{\rm gas}/L_B$
SALP-A	Salpeter [0.1–100]	5	0.47	Constant	0.95	0.79	1.54	0.55	1.14
SALP-B	Salpeter [0.1–100]	7	0.69	Constant	0.97	0.86	1.52	0.54	0.90
SALP-C	Salpeter [0.1–100]	10	1.3	$\propto R/h_B$	1.09	0.90	1.51	0.53	0.64
SALP-D	Salpeter [0.1–70]	10	1.8	$\propto R/h_B$ $(R<h_B)$; $\propto (R/h_B)^2$ $(R>h_B)$	1.19	0.78	1.58	0.53	0.51
SALP-E	Salpeter [0.09–100]	10	1.7	$\propto R/h_B$ $(R<h_B)$; $\propto (R/h_B)^2$ $(R>h_B)$	1.18	0.79	1.67	0.53	0.56
KROU-A	Kroupa [0.1–100]	2	0.75	Constant	1.07	0.32	1.37	0.69	0.56
KROU-B	Kroupa [0.2–100]	3	0.78	Constant	1.05	0.45	1.06	0.66	0.50
KROU-C	Kroupa [0.3–100]	4	0.75	Constant	0.99	0.61	0.84	0.63	0.47
KROU-D	Kroupa [0.35–100]	5	0.82	$\propto (R/h_B)^{1/2}$	1.02	0.73	0.73	0.60	0.43
KROU-E	Kroupa [0.4–100]	6	0.8	$\propto (R/h_B)^{1/2}$	0.99	0.84	0.66	0.58	0.42
KENN-A	Kennicutt [0.1–100]	3	0.21	Constant	0.80	0.84	0.75	0.55	1.06
KENN-B	Kennicutt [0.1–100]	4	0.25	Constant	0.80	0.93	0.73	0.53	0.95
KENN-C	Kennicutt [0.1–100]	5	0.29	Constant	0.81	1.02	0.71	0.62	0.86
KENN-D	Kennicutt [0–100]	4	0.32	Constant	0.88	0.82	0.92	0.55	0.93
KENN-E	Kennicutt [0–100]	5	0.38	Constant	0.89	0.89	0.90	0.54	0.84
KENN-F	Kennicutt [0–100]	7	0.49	Constant	0.89	1.00	0.87	0.53	0.72
KENN-G	Kennicutt [0.1–30]	5	0.61	Constant	0.96	0.78	0.74	0.56	0.50
KENN-H	Kennicutt [0.1–35]	7	0.61	Constant	0.92	0.97	0.69	0.53	0.51
KENN-I	Kennicutt [0.05–35]	5	0.54	Constant	0.94	0.81	0.79	0.56	0.58
KENN-J	Kennicutt [0.05–35]	7	0.78	$\propto (R/h_B)^{1/2}$	1.00	0.90	0.76	0.54	0.47
LARS-A	Larson [0.01–100]	1	0.085	Constant	0.70	0.82	0.84	0.51	2.25
LARS-B	Larson [0.01–100]	2	0.10	Constant	0.70	0.94	0.78	0.49	1.98
LARS-C	Larson [0.01–22]	5	0.60	$\propto (R/h_B)^{1/2}$	0.98	0.81	0.78	0.51	0.56
LARS-D	Larson [0.01–22]	6	0.79	$\propto (R/h_B)^{1/2}$	1.01	0.83	0.79	0.51	0.47
LARS-E	Larson [0.01–23]	7	0.68	$\propto (R/h_B)^{1/2}$	0.98	0.95	0.74	0.49	0.52
LMOD-A	mod. Larson [0.01–100]	4	0.54	Constant	0.97	0.68	0.97	0.59	0.67
LMOD-B	mod. Larson [0.01–100]	5	0.70	$\propto (R/h_B)^{1/2}$	1.01	0.74	0.93	0.57	0.58
LMOD-C	mod. Larson [0.01–100]	7	1.4	$\propto R/h_B$	1.10	0.77	0.95	0.56	0.39
LMOD-D	mod. Larson [0.2–100]	6	0.65	Constant	0.96	0.86	0.82	0.56	0.56
LMOD-E	mod. Larson [0.2–100]	7	0.78	$\propto (R/h_B)^{1/2}$	0.99	0.90	0.80	0.55	0.51
LMOD-F	mod. Larson [0.2–100]	8	0.92	$\propto (R/h_B)^{1/2}$	1.01	0.93	0.80	0.54	0.46
CHAB-A	Chabrier [0.01–100]	3	0.24	Constant	0.83	0.78	0.95	0.52	1.12
CHAB-B	Chabrier [0.01–100]	4	0.28	Constant	0.83	0.88	0.91	0.51	0.99
CHAB-C	Chabrier [0.01–100]	5	0.33	Constant	0.84	0.95	0.88	0.50	0.89
CHAB-D	Chabrier [0.01–32]	6	0.69	Constant	0.97	0.83	0.94	0.52	0.57
CHAB-E	Chabrier [0.01–32]	7	0.84	$\propto (R/h_B)^{1/2}$	1.01	0.87	0.91	0.51	0.51
CHAB-F	Chabrier [0.01–33]	8	0.92	$\propto (R/h_B)^{1/2}$	1.01	0.92	0.90	0.50	0.48

I luminosity in a comparable way. However, neglecting super-solar metallicities in the photometry has notable effects when considering, for instance, the B luminosity (Fig. 16). This is because the B band is both more sensitive to metallicity than the I band (Fig. 2) and more influenced by young stars, which have a metallicity that is higher on average and reaches super-solar values in the inner disc regions. Therefore, we stress the importance of covering the full metallicity range, from subsolar to super-solar metallicities, when computing the photometric properties of disc galaxies.

Fig. 17 shows the resulting gas-to-luminosity fraction $M_{\rm gas}/L_B$ for the chemo-photometric models, compared with the observational estimates for Sbc–Sc discs (Section 6.2). Models with the Salpeter IMF between 0.1 and 100 $\mathrm{M}_\odot$ (solid circles) tend to be too rich in gas with respect to observations. Considering that for a given set of stellar yields, the final metallicity increases with decreasing gas fraction (Tinsley 1980), our results indicate that with this IMF the global metal production (yield) is somewhat high: if we had imposed the models to reach the observed gas fractions, the final oxygen abundance in the gas would have been higher than observed. This finding is in line with known results for the solar neighbourhood: a Salpeter IMF extended up to 100 $\mathrm{M}_\odot$ produces too much oxygen to be compatible with the local evidence, while better agreement is found with an upper mass limit of 40–50 $\mathrm{M}_\odot$ (Tsujimoto et al. 1997; Thomas, Greggio & Bender 1998; Gratton et al. 2000).

The efficiency of metal enrichment from a stellar population can be estimated by computing the so-called global (or net) yield (Tinsley 1980; Pagel 1997):

$$y_Z = \frac{1}{\alpha}\int_{M(T)}^{M_{\rm s}} p_Z(M)\Phi(M)\,\mathrm{d}M, \qquad (5)$$

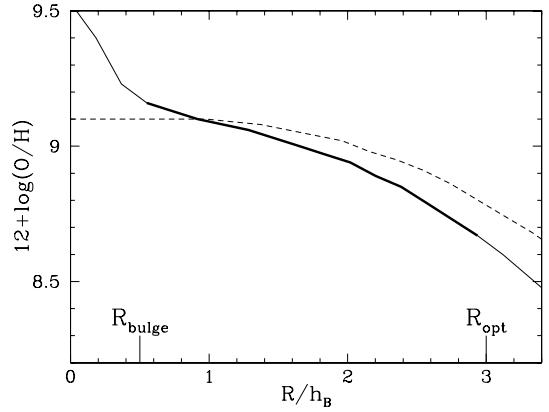

Figure 13. Metallicity gradient for model SALP-C, with radially increasing infall time-scale (Table 2), compared with a model with a constant infall time-scale $\tau_{\rm inf} = 10$ Gyr (dashed line). This figure is available in colour in the on-line version of the journal on *Synergy*.

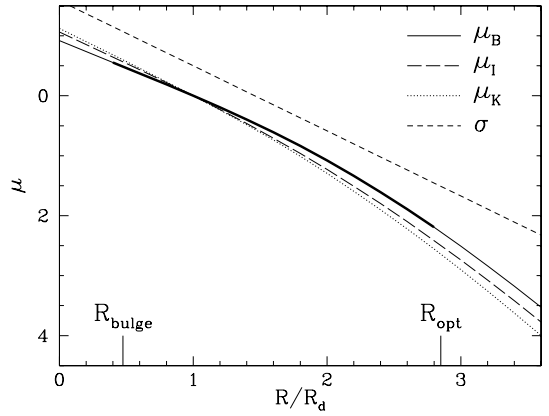

Figure 14. Surface brightness in B, I and K band for model SALP-A, all normalized to $\mu = 0$ at $R = R_{\rm d}$. The thick line marks the B-band profile in the significant 'disc region' between the bulge and the optical radius $R_{\rm opt}$ (see the text). Also shown is the underlying exponential mass profile $\sigma(R)$, vertically displaced by -0.5 for clarity. This figure is available in colour in the on-line version of the journal on *Synergy*.

where $M(T)$ is the stellar mass lifetime corresponding to the age T of the system (the galaxy) and $p_Z(M)$ is the mass fraction of new metals ejected by a star of mass M. Hence the integral expresses the amount of metals globally produced by a stellar generation over the age of the galaxy. The symbol α represents the fraction of mass locked up in 'ever-living' low-mass stars or remnants. In the instantaneous recycling approximation, the net yield can be directly used to predict the metallicity evolution (see Tinsley 1980; Pagel 1997 for details); with more complex chemical networks taking into account finite stellar lifetimes, delayed gas restitution and the different time-scales of release of different elements, as in our models, things are not as straightforward but the net yield per stellar generation still provides a useful insight into the efficiency of metal enrichment. In particular, it underlines that the latter does not depend merely on the amount of metals produced per mass involved in star formation, but on the ratio between this and the mass that remains forever locked in stars. The yield can thus be modified by altering the amount of metals produced (for instance, reducing/increasing the number of massive stars) and/or by changing the locked-up fraction.

For the Salpeter models, a lower yield seems to be necessary since oxygen is somewhat overproduced. We calculate model SALP-D, decreasing the upper-mass end $M_{\rm s}$ of the IMF to reduce the metal

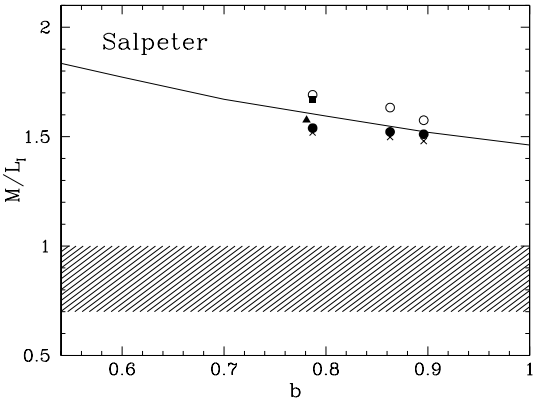

Figure 15. M/L ratio in the I band for chemo-photometric models with the Salpeter IMF. The shaded area marks the range $M/L_I = 0.7$–1 favoured by observations of Sbc–Sc discs ($b = 0.8$–1). Solid circles, models SALP-A-B-C adopting the standard IMF mass range [0.1–100] $\rm M_\odot$. Open circles, models SALP-A-B-C with photometry calculated at constant metallicity $Z = \rm Z_\odot = 0.019$. Crosses, models SALP-A-B-C with photometry calculated including only SSPs with $Z \leqslant \rm Z_\odot$. Triangle, model SALP-D with a smaller upper mass limit $M_{\rm s} = 70\ \rm M_\odot$. Square, model SALP-E with a smaller lower-mass limit $M_{\rm i} = 0.09\ \rm M_\odot$. Thin line, prediction from simple exponential models with $Z = \rm Z_\odot$. This figure is available in colour in the on-line version of the journal on *Synergy*.

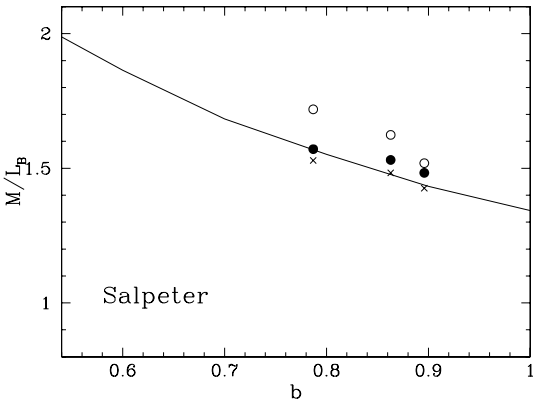

Figure 16. M/L ratio in the B band for chemo-photometric models with the Salpeter IMF. Symbols as in Fig. 15.

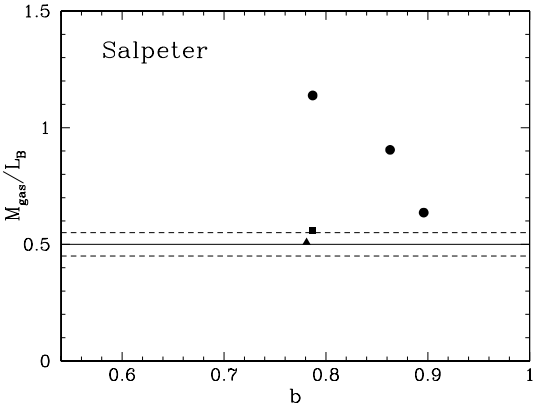

Figure 17. Gas-to-luminosity fraction for chemo-photometric models with the Salpeter IMF. Symbols as in Fig. 15. The horizontal lines mark the observational range of 0.5 ± 0.05 for the gas fraction in Sbc–Sc discs ($b =$ 0.8–1). This figure is available in colour in the on-line version of the journal on *Synergy*.

Table 3. Characteristic quantities for the IMFs adopted in the models of Table 2 (see the text). α is the locked-up fraction, $\zeta_{[1-2]}$ is the mass fraction in the [1–2] $M_\odot$ range, ζ_9 is the mass fraction in stars more massive than 9 $M_\odot$. y_O is the global oxygen yield of the IMF.

IMF	$[M_i - M_s]$	α	$\zeta_{[1-2]}/\alpha$	ζ_9/α	y_O
Salpeter	[0.1–100]	0.70	0.15	0.19	1.23E−02
Salpeter	[0.1–70]	0.71	0.15	0.17	1.16E−02
Salpeter	[0.09–100]	0.71	0.14	0.17	1.16E−02
Kroupa	[0.1–100]	0.71	0.23	0.10	7.05E−03
Kroupa	[0.2–100]	0.66	0.28	0.13	8.57E−03
Kroupa	[0.3–100]	0.62	0.34	0.15	1.03E−02
Kroupa	[0.35–100]	0.60	0.37	0.17	1.12E−02
Kroupa	[0.4–100]	0.58	0.40	0.18	1.23E−02
Kennicutt	[0.1–100]	0.56	0.34	0.27	1.82E−02
Kennicutt	[0–100]	0.61	0.28	0.22	1.47E−02
Kennicutt	[0.1–35]	0.58	0.35	0.19	1.51E−02
Kennicutt	[0.1–30]	0.59	0.35	0.18	1.39E−02
Kennicutt	[0.05–35]	0.60	0.32	0.18	1.39E−02
Larson	[0.01–100]	0.49	0.31	0.48	3.16E−02
Larson	[0.01–23]	0.55	0.32	0.24	1.75E−02
Larson	[0.01–22]	0.55	0.32	0.23	1.64E−02
Mod. Larson	[0.01–100]	0.63	0.28	0.17	1.13E−02
Mod. Larson	[0.2–100]	0.60	0.31	0.19	1.27E−02
Chabrier	[0.01–100]	0.59	0.26	0.24	1.62E−02
Chabrier	[0.01–33]	0.61	0.26	0.18	1.36E−02
Chabrier	[0.01–32]	0.61	0.26	0.17	1.34E−02

production, and obtain a corresponding gas fraction in agreement with observations (solid triangle in Figs 17 and 15). Alternatively, in model SALP-E we decrease the lower-mass end M_i and thereby increase the locked-up fraction, decrease the net metal yield and obtain again a gas fraction close to the observed values (solid square in Fig. 17).

Note, however, that, with the Salpeter IMF, a very restricted range of parameters (mass limits and infall time-scales) can yield an Sbc/Sc-type SFH ($b \sim 0.8$) together with metallicities and gas fractions both close to the observational values. What matters for the metallicity–gas fraction relation is in fact the yield, and models SALP-D and SALP-E have a similar oxygen yield (Table 3). However, when this condition is met by decreasing M_i (model SALP-E), the M/L ratio increases as we are shifting the IMF toward star masses that contribute no light (model SALP-E, solid square in Fig. 15).

7.2 Kennicutt models

The I-band M/L ratios of models KENN-A-B-C, adopting the Kennicutt IMF and standard limits [0.1–100] $M_\odot$, are shown as solid circles in Fig. 18 (upper panel); they lie close to the predictions from the simple exponential models of Section 5 (thin line) and within the range favoured by observations.

The lower panel shows that the corresponding gas-to-luminosity fractions M_{gas}/L_B are higher than observed, by a factor of 2 or so. Hence, the net yield of this IMF is also too high (see the discussion in the previous section for the Salpeter models). Although the slope at the high-mass end (−1.5) is steeper than in the Salpeter IMF, so that one might expect less massive stars and less oxygen production, for the bottom-light Kennicutt IMF the smaller number of low-mass stars results in a low locked-up fraction and hence a high net yield overall (Table 3). The slope at the low-mass end is so shallow that even extending the IMF down to $M_i = 0$ would increase the locked-up fraction only marginally, and would not improve the situation much (models KENN-D-E-F, open circles in Fig. 18). To reduce the global yield, the oxygen production per stellar generation must also be reduced, by lowering the high-mass end.

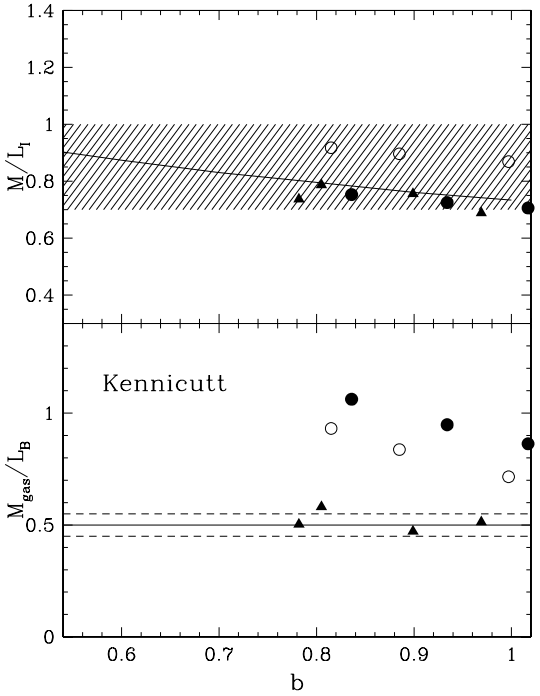

Figure 18. Upper panel, M/L ratio in the I band for chemo-photometric models with the Kennicutt IMF; lower panel, corresponding gas-to-luminosity fractions. The shaded area in the top panel and the dashed lines in the lower panel mark the observational ranges for Sbc–Sc discs (b = 0.8–1). Solid circles, models KENN-A-B-C adopting the standard IMF mass range [0.1–100] $M_\odot$. Open circles, models KENN-D-E-F adopting the lowest possible mass end, with range [0–100] $M_\odot$. Solid triangles, models KENN-G-H-I-J with mass limits tuned to reproduce the observed gas fractions (M_i = 0.05–0.1 $M_\odot$, M_s = 30–35 $M_\odot$). This figure is available in colour in the on-line version of the journal on *Synergy*.

In models KENN-G-H-I-J (triangles in Fig. 18) we tune the mass limits of the IMF so that we obtain an SFH typical of Sbc/Sc discs (b = 0.8–1) together with a suitable gas-to-luminosity fraction $M_{gas}/L_B \sim 0.5$. The corresponding M/L ratios are low, M/L_I = 0.7–0.8, still in agreement with the observed range.

7.3 Larson and Chabrier models

Models with the Larson or Chabrier IMF and mass limits [0.01–100] $M_\odot$ (LARS-A-B and CHAB-A-B-C in Table 2) have a low M/L ratio, in very good agreement with the corresponding simple models of Section 5; they are displayed as solid circles in Figs 19 and 20, respectively. However, in both cases the corresponding gas-to-luminosity fraction is exceedingly high, larger than the observed one by a factor of 2 for the Chabrier IMF and a factor of 4 for the Larson IMF. This again indicates that the global net yield is too high with these IMFs (Table 3). This is no surprise for the Larson IMF which has a Salpeter slope at high masses – and the Salpeter IMF already had a somewhat high oxygen yield, Section 7.1 – and in addition, due to the exponential cut-off at low masses, its locked-up fraction is much smaller, leading to a very high net yield. The Chabrier IMF is steeper at high masses, yet the low locked-up fraction produces a high yield.

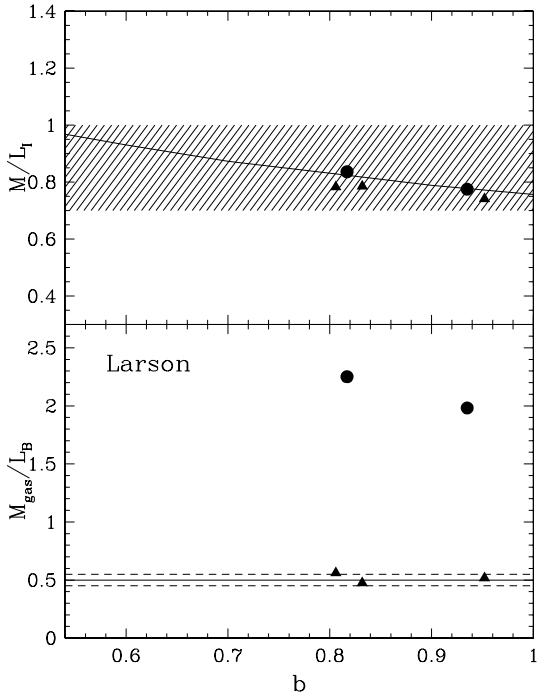

Figure 19. Upper panel, M/L ratio in the I band for chemo-photometric models with the Larson IMF; lower panel, corresponding gas-to-luminosity fractions. The shaded area in the top panel and the dashed lines in the lower panel mark the observational ranges for Sbc–Sc discs ($b = 0.8$–1). Circles, models LARS-A-B adopting the IMF mass range [0.01–100] $M_\odot$. Triangles, models LARS-C-D-E with upper mass limit tuned to reproduce the observed gas fractions ($M_s = 22$–23 $M_\odot$). This figure is available in colour in the on-line version of the journal on *Synergy*.

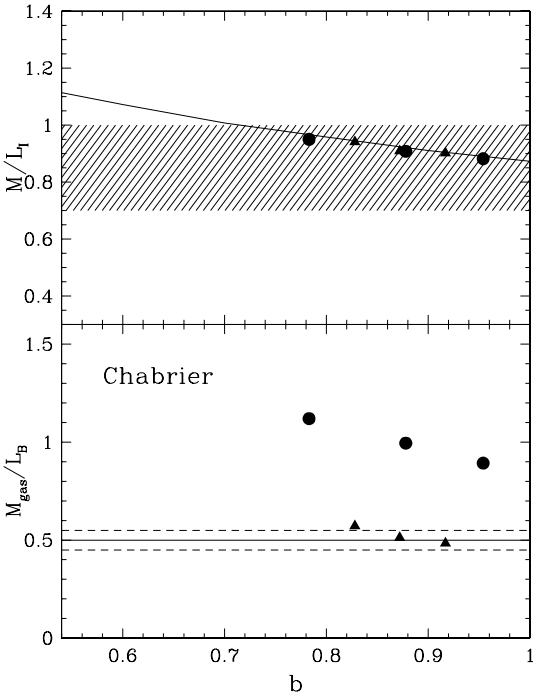

Figure 20. Same as in Figs 18–22 , but for the Chabrier IMF. Circles, models CHAB-A-B-C adopting the full IMF mass range [0.01–100] $M_\odot$. Triangles, models CHAB-D-E-F with upper mass limit $M_s = 32$–33 $M_\odot$, tuned to reproduce the observed metallicities and gas fractions with high-b parameters. This figure is available in colour in the on-line version of the journal on *Synergy*.

Both IMFs have a sharp cut-off at low masses, so that even reducing the low-mass end down to $M_i = 0$ has no effect on the locked-up fractions, and the only way to reduce the net yield is to lower the upper-mass end M_s. Models LARS-C-D-E with $M_s = 22$–23 $M_\odot$, and models CHAB-D-E-F with $M_s = 32$–33 $M_\odot$ reach the correct gas fraction, while the corresponding I-band M/L ratios are relatively unaffected by this tuning of the upper mass limits (triangles in Figs 19 and 20; see also Tsujimoto et al. 1997).

7.4 Kroupa and modified-Larson models

The Kroupa IMF and the modified-Larson IMFs are characterized by a rather steep slope of -1.7 for $M > 1$ $M_\odot$. Combined with the locked-up fractions corresponding to the standard mass limits of [0.1–100] $M_\odot$, such steep slopes result in low net yields compared with the IMFs previously considered, especially for oxygen which is produced in massive stars (Table 3). Actually, for the modified-Larson IMF the reference mass limits are [0.01–100] $M_\odot$, however, due to the sharp cut-off below the peak mass $\sim$0.25 $M_\odot$, changing the low-mass end of this IMF to $M_i = 0.1$ (or 0) $M_\odot$ has negligible effects on the results.

Consequently, with these IMFs the typical metallicities observed in disc galaxies can be obtained only for short infall time-scales, and correspondingly low-b parameters (models KROU-A and LMOD-A-B-C in Table 2, displayed as solid circles in Figs 21 and 22). Longer infall time-scales tend in fact to dilute the metals produced and lower the final metallicity, for a given net yield.

To reach higher b-values ($b = 0.8$–1), longer infall time-scales are required; at the same time, the net yield must be increased to reproduce the typical oxygen abundance of 9.1 dex at $R = h_B$. This

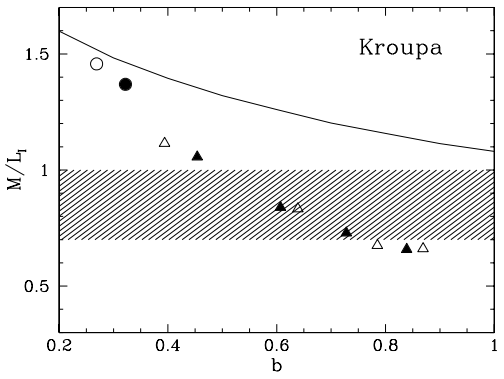

Figure 21. M/L ratio in the I band for chemo-photometric models with the Kroupa IMF. The shaded area marks the range $M/L_I = 0.7$–1 favoured by observations of Sbc–Sc discs ($b = 0.8$–1). Circles, models adopting the standard IMF mass range [0.1–100] $M_\odot$; they lie quite close to the predictions from the exponential models from Section 5 (thin line). Triangles, models adopting a higher low-mass end $M_i = 0.2$–0.4 to reproduce the observed metallicities at higher b-values; the M/L ratio correspondingly decreases because of the lower locked-up fraction. Solid symbols, models KROU-A-B-C-D-E listed in Table 2, with a gas-to-luminosity fraction $M_{gas}/L_B \sim 0.5$. Open symbols, other calculated models, with slightly different gas fraction. This figure is available in colour in the on-line version of the journal on *Synergy*.

we can achieve by increasing the lower-mass end M_i, which corresponds to decreasing the locked-up fraction and also the M/L ratio with respect to the standard case.

As to the Kroupa case, models KROU-B-C-D-E correspond to increasing values of the b parameter (solid triangles in Fig. 21). For simplicity, in Table 2 we list only Kroupa models with a

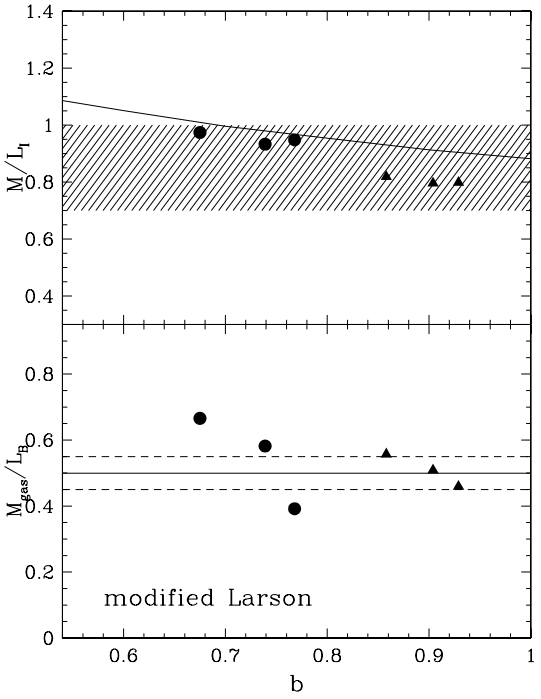

Figure 22. Same as in Figs 18–20 , but for the modified Larson IMF. Circles, models LMOD-A-B-C adopting the full IMF mass range [0.01–100] $M_\odot$. Triangles, models LMOD-D-E-F with a lower-mass limit of $M_i = 0.2\ M_\odot$, tuned to reproduce the observed metallicities and gas fractions with high-b parameters. This figure is available in colour in the on-line version of the journal on *Synergy*.

gas-to-luminosity fraction close to the observed value $M_{gas}/L_B \sim 0.5$ (solid symbols in Fig. 21); other models with slightly different gas fractions (open symbols) do not appreciably change the trends of the M/L ratios versus the b parameter. A good Sbc/Sc model ($b \sim 0.85$) is KROU-E, but such high values of b, combined with the constraints on oxygen production, are reached only with an uncomfortably large $M_i = 0.4\ M_\odot$. This limit, however, should not be taken at face value: a sharp cut-off at low masses is just a simplistic way to reduce the locked-up fraction so as to increase the yield. Stars below $\sim 0.8\ M_\odot$ do not contribute metals nor substantial luminosity, and for chemical and photometric evolution their mass distribution is irrelevant, what matters is just their global mass. Any other distribution of masses at the low-mass end, with the same locked-up fraction, would leave our results unchanged (see also Tsujimoto et al. 1997). Not surprisingly, with such a low locked-up fraction, the resulting M/L ratio is very low ($\lesssim$0.7, Fig. 21).

For the modified-Larson IMF, the net yield is larger than in the Kroupa case, thanks to the exponential cut-off at low masses and the correspondingly lower locked-up fraction (for the same mass limits). In this case, a less extreme value of the low-mass end $M_i = 0.2\ M_\odot$ suffices to reproduce the observed metallicities and gas-to-luminosity fractions with $b \geqslant 0.8$; the resulting typical M/L ratio is $\sim$0.8 (Fig. 22).

In conclusion, the Kroupa and modified-Larson IMFs, adopting a steep Scalo slope of -1.7 for $M \gtrsim 1\ M_\odot$, seem to encounter the opposite problem compared with the IMFs previously discussed: they are too inefficient in terms of oxygen production to account easily for the observed metallicities in spirals, if an SFH of the type of Sbc/Sc discs is required at the same time ($b > 0.8$). See, however, Kroupa (2001) concerning the uncertainties on the slope of the IMF at high masses: a value shallower than 1.7, possibly up to the Salpeter slope $\sim$1.3, is by no means excluded from local observations.

7.5 An overview of the results

For all the IMF considered, the full chemo-photometric models lie close to the predictions of the corresponding simple models with the same mass limits – a complex result of combining realistic, infall-like and radially dependent SFHs with metallicity-dependent photometry. Consequently, the conclusions of Section 5 for the M/L ratios are confirmed.

The Salpeter IMF results in M/L ratios much higher than required to match observations; moreover, a Salpeter slope over the whole stellar mass range is currently not supported by observations (see Section 1). As to the bottom-light IMFs, broadly speaking we see two types of behaviour.

In the first case the low locked-up fraction typical of bottom-light IMFs leads to a high global yield (Kennicutt, Larson and Chabrier models), too high to reproduce the typical gas fractions of Sbc/Sc spirals at the same time as their metallicities. These IMFs have yields comparable to what is required to explain the observed metal enrichment of hot gas in galaxy clusters ($y \sim 2$–$3\ Z_\odot$, Pagel 2002), and much higher than what is typically inferred for the solar neighbourhood ($y \lesssim Z_\odot$) – compare the oxygen yields y_O in Table 3 with the solar oxygen abundance $Z_{O,\odot} \sim 9 \times 10^{-3}$. A possible explanation is that disc galaxies, just like ellipticals in clusters, disperse a large part of the metals they produce into the intergalactic medium, so that we do not detect these metals in present-day discs. Blow-out of material from present-day discs is observed in the form of fountains, but this gas does not seem to have the necessary energy to escape the galactic potential, so that it just falls back on to the disc on relatively short time-scales ($\sim 10^8$ yr, Bregman 1980; Fraternali et al. 2001; Heckman 2002). So, escape of large quantities of metals from present-day discs does not seem very realistic. However, in the early phases of galaxy formation it is possible that dispersal of metals took place, when the potential well of the galaxy was weaker; large outflows are in fact observed in high-redshift Lyman-break galaxies, though these are usually identified with the progenitors of ellipticals (Pettini et al. 2000). Besides, there are arguments advocating large outflows of baryons from galaxies in general (Silk 2003).

Alternatively, a large part of the metals produced may be locked-up in dust, which may correspondingly induce an observational underestimate of the true metallicity in spiral galaxies. Theoretical models and observational evidence suggest that in the interstellar medium of our Galaxy, 40 per cent of the metals is locked-up in dust grains (Dwek 1998 and references therein). Consequently, the oxygen abundance probed by atomic emission lines might be underestimated by almost a factor of 2. However, the oxygen abundance is typically measured in H II regions, where dust depletion is probably much lower than the average for the diffuse interstellar medium; besides, oxygen abundances and abundance gradients derived from the spectra of OB stars, which should be totally unaffected by dust depletion, agree very well with those from H II regions (Smartt & Rolleston 1997; Gummersbach et al. 1998). So we consider oxygen abundances measured in H II regions as a reliable estimate of the real metallicity of a galaxy. Dust depletion does not seem to provide a viable solution to the apparent overproduction of metals.

As an alternative solution to metal outflows, some fine-tuning of the upper mass limit of the IMF can be applied, corresponding to a tuning of the global yield, so that the chemical properties of discs

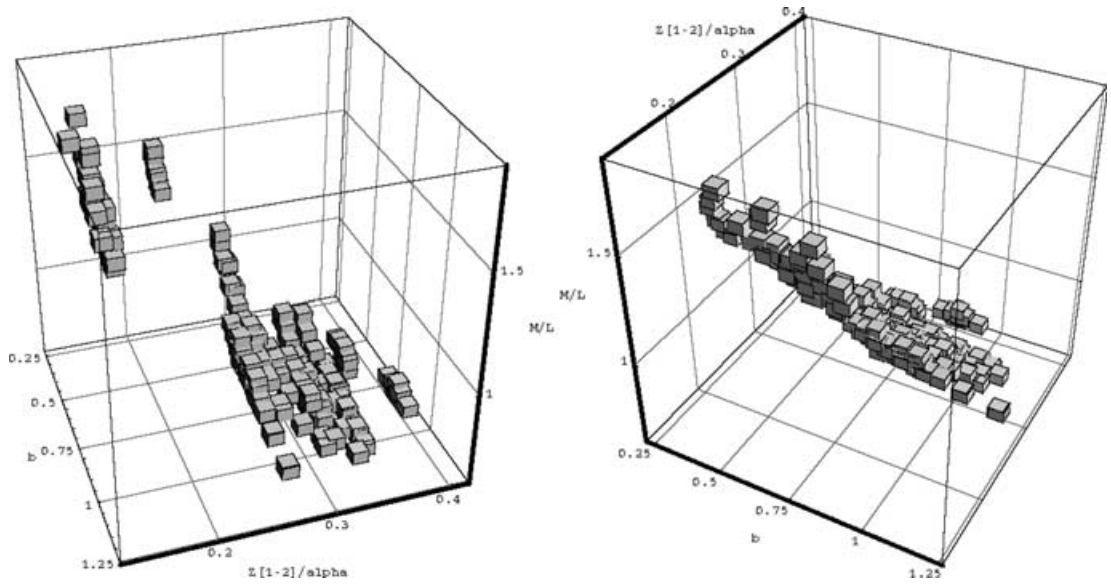

Figure 23. 3D plot relating the M/L_I ratio to the b parameter and to the IMF 'driving quantity' $\zeta_{[1-2]}/\alpha$ (see the text). This figure is available in colour in the on-line version of the journal on *Synergy*.

can be matched without requiring considerable dispersal of metals.[4] However, the resulting I-band M/L ratio is quite robust to such fine-tuning (see Section 7.6 and Tsujimoto et al. 1997), and for Sbc/Sc discs we consistently find for these IMFs $M/L_I < 1$, with values between 0.7 (Kennicutt IMF) and 0.9 (Chabrier IMF).

In the second category, we find IMFs with a steep slope at the high-mass end (-1.7, Kroupa and modified-Larson IMFs) implying a low oxygen yield. In this case, to reproduce the observed metallicities and gas fractions combined with an Sbc/Sc-like SFH ($b \geqslant 0.8$) the global yield must be increased, via reducing the locked-up fraction with a higher minimum stellar mass $M_{\rm i}$. Correspondingly, since less mass is locked in very low-mass, low-luminosity stars, the M/L ratio also decreases, and for the Kroupa and modified-Larson models of Sbc/Sc galaxies we find again $M/L_I \sim 0.7$–0.8.

Our conclusions derived from the 'chemical properties' of discs, i.e. the typical metallicities and gas fractions, are still subject to some uncertainties. The constraint of the gas-to-luminosity fraction is rather uncertain as it has been derived by assembling a number of independent studies and by applying various corrections (see Section 6.2); besides, it relies on the B luminosity, which is affected by uncertain dust extinction. Furthermore, the global yield of a given IMF, and the corresponding fine-tuning of the mass limits necessary in chemical models, depends on the adopted stellar yields; here also some uncertainties exist, although the present study is mainly based on oxygen, which is the element with best estimated theoretical yields. However, the M/L ratio is generally robust with respect to the fine-tuning of the IMF mass limits we applied to reproduce metallicities and gas fractions. For a metallicity distribution resembling the observed one (oxygen abundance of approximately 9.1 dex at $R = h_B$, gradient around -0.2 dex kpc^{-1}) we obtain $M/L_I = 0.7$–0.9 as a consistent result for Sbc/Sc disc models, with all the bottom-light IMFs we considered. Many other models were computed than those presented here, with shallower or steeper gradients (say, between -0.1 and -0.3 dex kpc^{-1}), or typical metallicities slightly different from the reference value of 9.1 (say between 9.0 and 9.2), and the conclusions on the M/L ratio in the I band for late-type discs are quite robust to such variations in the model constraints.

[4] The same reduction of the net yield is obtained, if above a certain stellar mass there is fallback of metals on to a central black hole after the supernova explosion (Colpi, Shapiro & Wasserman 1996; Zampieri, Shapiro & Colpi 1998; MacFadyen, Woosley & Heger 2001; Podsiadlowski et al. 2002). In the presence of fallback, the actual amount of metals enriching the interstellar medium is less than what is formally predicted by supernova models. See also Tsujimoto et al. (1997).

7.6 The driving parameters for the M/L ratio

We have demonstrated that various 'bottom-light' IMFs suggested in recent literature result in low M/L ratios $M/L_I < 1$ for Sbc/Sc discs. It is interesting to discuss what is the common feature, among these different IMFs, that determines this result.

We analysed in our models the correlations between the predicted M/L ratio and various quantities characterizing the IMF, e.g. the mass fraction in stars around $1\,{\rm M}_\odot$, or around $10\,{\rm M}_\odot$, or the mass fraction in 'ever-living' stars below $1\,{\rm M}_\odot$, etc. The best correlation is found with the quantity $\zeta_{[1-2]}/\alpha$, where $\zeta_{[1-2]}$ is the mass fraction that a given IMF 'assigns' to stars between 1 and $2\,{\rm M}_\odot$ and α is the mass fraction that remains locked in ever-living stars and remnants. Fig. 23 shows a three-dimensional (3D) plot of the resulting M/L_I as a function of the b parameter and of the above-mentioned quantity $\zeta_{[1-2]}/\alpha$ characterizing the IMF. The plot shows the 'calibrated' models in Table 2, and many other models with a variety of IMF mass limits, metallicities, gas-to-luminosity fractions, etc., run during the calibration process. Besides the expected dependence on the b parameter amply discussed in this paper, the typical M/L_I evidently decreases at increasing $\zeta_{[1-2]}/\alpha$. Fig. 24 underlines the latter dependence by showing a 'slice' of the 3D plot of Fig. 23, corresponding to large b parameters $b \geqslant 0.7$ and projected on the $(\zeta_{[1-2]}/\,\alpha, M/\,L_I)$ plane. These correlations indicate that, in general, the M/L_I ratio is lower when the IMF favours stars in the [1–2] ${\rm M}_\odot$ range versus stars of lower masses and remnants from more massive stars.

This 'driving quantity' $\zeta_{[1-2]}/\alpha$ is relevant for the M/L ratio in red optical bands such as the I band. At different wavelengths, the

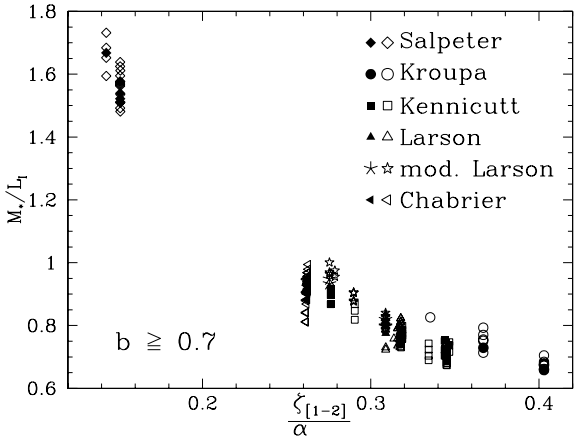

Figure 24. Relation between M/L_I and the 'driving quantity' $\zeta[1-2]/\alpha$ (see the text), for models with $b \geqslant 0.7$. Solid symbols for the 'calibrated' models in Table 2, open symbols for other models. A given IMF-symbol can correspond to different values of the abscissa because the models explore different mass limits (cf. Table 2). This figure is available in colour in the on-line version of the journal on *Synergy*.

luminosity is dominated by stars of different masses and the corresponding IMF–M/L ratio relation is driven by a different quantity. For instance, a similar analysis of the M/L ratio in the B band shows that this is influenced mostly by the mass fraction in the range [1–9] $M_\odot$, as expected from the fact that B-band light is sensitive to the contribution of more massive stars.

For the IMFs and the corresponding mass limits in the calibrated models of Table 2, we list the characteristic quantities $\zeta_{[1-2]}$, α, etc. in Table 3. We also list the global oxygen yield y_O (see equation 5) and the related IMF quantity ζ_9/α, where ζ_9 is the mass fraction in stars more massive than 9 $M_\odot$ – since it is these stars that contribute the bulk of the oxygen production. Actually, stellar yields depend on metallicity and this effect is included in our chemical models (Portinari et al. 1998); the global yields and locked-up fractions listed for illustration in Table 3 are computed for solar metallicity.

Traditionally, in chemical models the stellar IMF has been characterized by the quantity ζ_1, that is the mass fraction in stars more massive than 1 $M_\odot$. This corresponds to dividing the IMF into two mass ranges, the 'ever-living' low-mass stars, locking up mass out of further chemical processing forever, and stars with a lifetime shorter than a Hubble time that recycle gas and metals; this description is useful and meaningful within the simplified instantaneous recycling approximation for chemical evolution. A similar approach is also applied when deriving the IMF from the present-day mass function (PDMF), grossly separating ever-living stars, the PDMF of which is the integrated result of the IMF over the history of the galaxy, from stars with finite stellar lifetimes then assumed to evolve 'instantly', the PDMF of which is a direct signature of the IMF (Tinsley 1980; Scalo 1986).

In the light of our results for the M/L ratio, we suggest a gross description of the IMF based on three mass ranges. (i) Ever-living stars ($M \lesssim 0.8$–1 $M_\odot$) contribute to the locked-up fraction; their contribution to luminosity becomes important only for very old systems, where they are not much smaller than the typical 'turn-off mass'. (ii) Intermediate living stars ($M \sim 1$–9 $M_\odot$) contribute an important amount of recycled gas (for a Salpeter IMF, ∼two-thirds of the total returned gas fraction) and dominate the luminosity; depending on the observational band considered, the 'important' subrange for the luminosity may change: e.g. [1–2] $M_\odot$ for the I band, [1–9] $M_\odot$ for the B band. (iii) Short-lived stars ($M > 9$ $M_\odot$) contribute part of the recycled gas, part of the locked-up fraction (through the remnants) and most of the metals (oxygen, in particular); their luminosity contribution is dominant only for blue and UV bands, and/or for very young systems or systems dominated by a recent burst. Here we prefer the terminology 'ever-, intermediate- and short-living' stars rather than 'low-, intermediate- and high-mass' stars, to distinguish this classification from the mass ranges classified on the basis of stellar evolution properties (Iben 1991; Chiosi, Bertelli & Bressan 1992).

Broadly speaking, it is the relative proportion of the mass fractions in these three ranges that determines the expected chemo-photometric properties of the system. Since for the I band, the mass range dominating the luminosity differs from the mass range responsible for the oxygen production, it is easy to understand how we could tune the yields through the IMF upper mass limits and reproduce the observed gas-to-luminosity fraction, with negligible effects on the M/L_I ratio (Section 7.5; see also Tsujimoto et al. 1997). However, this dichotomy may not hold when one consider other bands (for instance, blue or UV bands more sensitive to the contribution of massive stars) or other chemical elements (for instance, helium, carbon, nitrogen and iron, produced in non-negligible amounts by 'intermediate living' stars, including SN Ia). In contrast, one can envisage a connection between the M/L ratio in certain bands and the production of certain elements. So for a full account of the chemo-photometric evolution of galaxies, it is important to maintain consistency between the computed luminosity and chemical outputs (Marigo & Girardi 2001).

7.7 The total baryonic M/L ratio

In this section we discuss the global baryonic M/L ratio, including the mass in gas, for those models of Sbc/Sc discs (large b values) that also comply with the constraint on the gas-to-luminosity ratio (Section 6.2) – and hence have the amount of gas indicated by observations.

With the Salpeter IMF, the typical global baryonic M/L ratio in Sbc/Sc discs is $\gtrsim 2$ $M_\odot/L_\odot$ (Table 4, column 5), and the mass in gas is approximately 25 per cent of the total baryonic mass (column 6). With the bottom-light IMFs, the gas contribution is more important since less mass is stored in the stellar component, for the same luminosity. With the adopted gas-to-luminosity ratio, the gas mass typically accounts for 40 per cent of the total baryonic mass in Sbc/Sc discs, and the global baryonic M/L ratio is 1.2–1.5 $M_\odot/L_\odot$.

A gas fraction of 40 per cent may seem exceedingly large, but here we are dealing with late-type spirals, which are notoriously gas-rich (Roberts & Haynes 1994; Sommer-Larsen 1996). Besides, the gas fraction is a strong function of radius: in the inner parts, say within $R < 1h_B$, our Sbc/Sc models typically have a gas fraction of less than 20 per cent, increasing at higher radius. So, while the gas mass is relevant in computing the global baryonic mass in the disc, in the inner regions the baryonic content is definitely dominated by the stellar component.

Besides, we find that the face-value gas fractions depend on the adopted gas-to-luminosity ratio, suggested from observations that are as yet rather uncertain (Section 6.2). This section is just meant to draw attention on the fact that, with bottom-light IMFs, the gas mass is likely to contribute significantly to the total baryonic mass in late-type discs, and it should not be neglected when estimating the global baryonic content. This may be crucial when discussing the physical nature of the Tully–Fisher relation, since over a wide

Table 4. Total baryonic M/L ratio of the model Sbc/Sc discs from Table 2, including the mass in gas. (1) Model name. (2) Adopted IMF with corresponding mass limits. (3) b parameter of the SFH (equation 4). (4) M/L ratio in the I band of the stellar component (comprehensive of living stars and stellar remnants). (5) Total baryonic M/L ratio including the gas mass: $M_{\rm bar} = M_* + M_{\rm gas}$. (6) Gas mass fraction in the baryonic disc.

(1) Model	(2) IMF	(3) b	(4) M_*/L_I	(5) $M_{\rm bar}/L_I$	(6) $M_{\rm gas}/M_{\rm bar}$
SALP-D	Salpeter [0.1–70]	0.78	1.58	2.09	0.24
SALP-E	Salpeter [0.09–100]	0.79	1.67	2.23	0.25
KROU-D	Kroupa [0.35–100]	0.73	0.73	1.12	0.35
KROU-E	Kroupa [0.4–100]	0.84	0.66	1.06	0.38
KENN-G	Kennicutt [0.1–30]	0.78	0.74	1.22	0.40
KENN-H	Kennicutt [0.1–35]	0.97	0.69	1.21	0.43
KENN-I	Kennicutt [0.05–35]	0.81	0.79	1.35	0.42
KENN-J	Kennicutt [0.05–35]	0.90	0.76	1.23	0.39
LARS-C	Larson [0.01–22]	0.81	0.78	1.37	0.43
LARS-D	Larson [0.01–22]	0.83	0.79	1.28	0.39
LARS-E	Larson [0.01–23]	0.95	0.74	1.30	0.43
LMOD-D	mod. Larson [0.2–100]	0.86	0.82	1.36	0.40
LMOD-E	mod. Larson [0.2–100]	0.90	0.80	1.30	0.39
LMOD-F	mod. Larson [0.2–100]	0.93	0.80	1.26	0.36
CHAB-D	Chabrier [0.01–32]	0.83	0.94	1.53	0.38
CHAB-E	Chabrier [0.01–32]	0.87	0.91	1.45	0.37
CHAB-F	Chabrier [0.01–33]	0.92	0.90	1.42	0.36

enough dynamical range the rotation velocity appears to correlate better with the global baryonic (stars+gas) mass, rather than with the stellar mass only (McGaugh et al. 2000). When discussing the baryonic TF relation, the M/L ratio ascribed to the stars and, correspondingly, the relative contribution of the gas mass have important consequences for the derived slope (McGaugh 2001, 2003). Lower-than-Salpeter M/L ratios, as favoured in the present paper, imply a somewhat shallower TF relation (Bell & de Jong 2001; de Jong & Bell 2001).

7.8 An indirect comparison to the solar neighbourhood

Tsujimoto et al. (1997, hereinafter T97) performed an analogous study to our present one, combining chemical evolution and M/L ratio constraints for the solar neighbourhood to determine a three-parameter IMF. Although their study was similar in spirit to ours, it is not trivial to compare results, both because of substantial differences in the models (in stellar yields, SN Ia rate formalism, SF law and photometric computations) and because of the different approach (detailed chemical patterns and star counts in the solar neighbourhood, versus global average properties of external Sbc/Sc disc galaxies). Still, a comparison can be interesting and we shall broadly outline it.

T97 considered single-slope IMFs with varying mass limits so that their set of IMF parameters is ($M_{\rm i}$, $M_{\rm s}$, x), where x is the power-law slope. A direct comparison with our results is possible for the 'power-law IMFs' considered in this paper (Salpeter, Kroupa and Kennicutt): although the Kroupa and Kennicutt IMFs are not single-slope, the slope changes only below 1 $M_\odot$ where what matters is effectively the global mass in low-mass stars, rather than the detailed mass distribution (T97 and Section 7.4). For our 'best models' of Sbc/Sc discs listed in Table 4, with the right gas-to-luminosity ratio (i.e. right level of metal enrichment), we can compute the 'equivalent' value of $M_{\rm i}$ that, for a single-slope IMF, would result in the same mass fraction below 1 $M_\odot$ ($M_{\rm i,eq}$ in Table 5). We also compare the mass fractions within the three significant mass ranges discussed in Section 7.6: 'ever-living' ($M < 1$ $M_\odot$), intermediate-living ($M = 1$–$9\,M_\odot$) and short-lived ($M > 1$ $M_\odot$) stars. In Table 5 we list the various IMF parameters as constrained by T97 and in this paper. For brevity, we consider the highest values of $M_{\rm s}$ and of $M_{\rm i}$ allowed in Fig. 3 of T97; considering their lower values somewhat increase the discrepancy with our results (see below), but does not change the outcome of this qualitative comparison.

For each of the IMFs in Table 5, our results favour smaller low-mass fractions $\zeta_{<1}$, and higher fractions both in the intermediate [1–9] $M_\odot$ and in the high >9 $M_\odot$ mass range. This implies both a higher metal enrichment (roughly driven by $\zeta_{>9}/\alpha$ or $\zeta_{>9}/\zeta_{<1}$) and a lower M/L ratio (roughly driven by $\zeta_{[1-9]}/\zeta_{<1}$) in our models. The higher level of metal enrichment might be related to the fact that the gas-to-luminosity ratio of external spirals is certainly a more uncertain and loose constraint on chemical evolution than the detailed abundance patterns in the solar neighbourhood considered by T97. For instance, a very recent compilation (Bettoni, Galletta & García-Burillo 2003) seems to favour lower gas fractions ($M_{\rm HI}/L_B \sim 0.2$ and $M_{\rm H_2}/L_B \sim 0.1$) than we adopted in Section 6.2, which would correspond to a lower efficiency of metal enrichment for external spirals. In the context of our models, this could be obtained via a different tuning of the upper mass limit $M_{\rm s}$ of the IMF to reduce the characteristic yield, but as discussed in Sections 7.5 and 7.6 the resulting M/L ratios would hardly change.

As to the different M/L ratio between T97 and this paper, it is difficult to understand whether the discrepancy is due to model differences or to the different approach (solar neighbourhood versus external discs). The difference is not simply accounted for by different SFHs, since both the solar neighbourhood in T97 and the Sbc/Sc discs here have been modelled with the respective suitable SFHs. Possibly, while chemical evolution is much better constrained in the solar neighbourhood, the estimate of the local luminosity from star counts (T97) is more cumbersome than the study of the global luminosity in external galaxies. Besides, dark matter may have a

Table 5. Comparison between IMFs as constrained by T97 and in the present paper (PST). $M_{\rm i}$ and $M_{\rm s}$ are the mass limits of the IMF of slope x; $\zeta_{<1}$, $\zeta_{[1-9]}$ and $\zeta_{>9}$ are the corresponding mass fractions in the three representative mass ranges. $M_{\rm i}^{\rm eq}$ (PST) is the 'single-slope equivalent' lower-mass limit for our IMFs (see the text). (*) Slopes $x > 1.6$ are formally ruled out by T97, because for steep slopes they find that no value of $M_{\rm i}$ can fulfil both the chemical and the M/L ratio constraints. Still, for qualitative comparison with our Kroupa models we consider their case $x = 1.7$ with $M_{\rm i} = 0.23$, an intermediate value between those allowed by chemical and M/L ratio arguments (Fig. 3 in T97).

IMF	x	$M_{\rm i}^{\rm T97}$	$M_{\rm s}^{\rm T97}$	$\zeta_{<1}^{\rm T97}$	$\zeta_{[1-9]}^{\rm T97}$	$\zeta_{>9}^{\rm T97}$	$M_{\rm i,eq}^{\rm PST}$	$M_{\rm s}^{\rm PST}$	$\zeta_{<1}^{\rm PST}$	$\zeta_{[1-9]}^{\rm PST}$	$\zeta_{>9}^{\rm PST}$
Salpeter	1.35	0.05	50	0.71	0.21	0.08	0.09–0.1	70–100	0.62	0.26	0.12
Kennicutt	1.5	0.14	55	0.66	0.26	0.08	0.35–0.38	30–35	0.44	0.45	0.11
–	1.6	0.17	58	0.68	0.26	0.06	–	–	–	–	–
Kroupa(*)	1.7	0.23	64	0.65	0.29	0.06	0.44–0.47	100	0.44	0.46	0.10

minor, but non-zero contribution to the local dynamical M/L ratio, easing the M/L constraints adopted by T97. Alternatively, the discrepancy might be resolved when, for the M/L ratio of external galaxies, allowance is made for the dispersion and the uncertainty in the zero-point of the TF relation (Appendix A).

The issue deserves further investigation, but this is beyond the purpose of this paper. Reasonably, one should first assess whether there is an effective discrepancy in the observationally deduced M/L ratio and the IMF, free from modelling issues. The two environments, the solar neighbourhood and outer disc galaxies, should be analysed with the same models so that a significant comparison can be made. We postpone to future work the study of the M/L ratio and IMF in the solar neighbourhood with our chemo-photometric models.

8 THE BULGE CONTRIBUTION

In this section we attempt to give a rough estimate of the contribution of the bulge to the global M/L ratio of disc galaxies. Bulges tend to be older and dimmer than discs, although in some cases a continuity of properties (colours, etc.) is seen between the bulge and the inner regions of the disc, especially for late-type spirals (Balcells 2003 and references therein). A lower limit to the global M/L ratio is hence given by considering the central regions as the extrapolation of the disc properties to the centre, which is included in our models. As described in Section 6.3, from the analysis of our disc models we had excluded the inner regions ($R \leqslant 0.5\, h_B$); including them yields the M/L ratios in parentheses in column 4 of Table 6. We limit the list to models with large b parameters, as representative of Sbc/Sc spirals. The inclusion of the central disc regions induces a minor increase (at most 10 per cent) in the global M/L ratio. In particular, for all the 'bottom-light' IMFs considered, the M/L ratio remains below 1 for the Sbc/Sc models.

An upper limit to the bulge M/L ratio is given by the characteristic M/L ratio of an old SSP, neglecting any possible tails of later star formation and younger stellar components – expected among others because of gas recycling from the first population, and detected for instance in the bulge of the Milky Way (Ng et al. 1995; van Loon

Table 6. Estimated bulge contribution, total $(M/L)_I$ ratios and K-band $\mathcal{B}/\mathcal{D}$ ratios for the Sbc/Sc models of Table 2. (1) Model name. (2) Adopted IMF with corresponding mass limits. (3) b parameter of the SFH (equation 4). (4) M/L ratio in the I band of the stellar component in the disc; in parentheses the M/L ratio when considering the disc extended to the Galactic Centre. (5) Stellar M/L_I ratio of a SSP of solar metallicity and age 10 Gyr, representing the bulge, with the IMF indicated in column 2. (6) Actual mass ratio between the disc and a bulge with I-band luminosity 25 per cent of that of the disc. (7) Global galactic M/L_I ratio assuming a 10 Gyr old bulge with $(\mathcal{B}/\mathcal{D})_I = 25$ per cent. (8) M/L ratio in the K band of the stellar component in our disc models. (9) Stellar M/L_K ratio of a SSP of solar metallicity and age 10 Gyr, representing the bulge, with the IMF indicated in column 2. (10) $\mathcal{B}/\mathcal{D}$ luminosity ratio in the K band corresponding to the mass ratio in column 6, or equivalently to the adopted $(\mathcal{B}/\mathcal{D})_I = 25$ per cent.

(1) Model	(2) IMF	(3) b	(4) $M_*/L_I(\mathcal{D})$		(5) $M_*/L_I(\mathcal{B})$	(6) $M_*(\mathcal{B})/M_*(\mathcal{D})$	(7) M_*/L_I(tot)	(8) $M_*/L_K(\mathcal{D})$	(9) $M_*/L_K(\mathcal{B})$	(10) $(\mathcal{B}/\mathcal{D})_K$
SALP-A	Salpeter [0.1–100]	0.79	1.54	(1.60)	3.77	0.61	1.99	0.67	1.31	0.31
SALP-B	Salpeter [0.1–100]	0.86	1.52	(1.57)	3.77	0.62	1.97	0.65	1.31	0.31
SALP-C	Salpeter [0.1–100]	0.90	1.51	(1.62)	3.77	0.62	1.96	0.64	1.31	0.30
SALP-D	Salpeter [0.1–70]	0.78	1.58	(1.68)	3.76	0.59	2.02	0.66	1.31	0.30
SALP-E	Salpeter [0.09–100]	0.79	1.67	(1.71)	3.99	0.60	2.13	0.70	1.38	0.30
KROU-D	Kroupa [0.35–100]	0.73	0.73	(0.77)	1.53	0.52	0.89	0.31	0.53	0.31
KROU-E	Kroupa [0.4–100]	0.84	0.66	(0.68)	1.41	0.53	0.81	0.28	0.49	0.31
KENN-A	Kennicutt [0.1–100]	0.84	0.75	(0.77)	1.80	0.60	0.96	0.33	0.61	0.32
KENN-B	Kennicutt [0.1–100]	0.93	0.73	(0.74)	1.80	0.62	0.94	0.32	0.61	0.32
KENN-C	Kennicutt [0.1–100]	1.02	0.71	(0.72)	1.80	0.63	0.93	0.31	0.61	0.32
KENN-D	Kennicutt [0–100]	0.82	0.92	(0.95)	2.23	0.61	1.18	0.35	0.76	0.28
KENN-E	Kennicutt [0–100]	0.89	0.90	(0.93)	2.23	0.62	1.17	0.34	0.76	0.28
KENN-F	Kennicutt [0–100]	1.00	0.87	(0.89)	2.23	0.64	1.14	0.33	0.76	0.29
KENN-G	Kennicutt [0.1–30]	0.78	0.74	(0.76)	1.78	0.60	0.95	0.31	0.61	0.31
KENN-H	Kennicutt [0.1–35]	0.97	0.69	(0.71)	1.79	0.65	0.91	0.30	0.61	0.32
KENN-I	Kennicutt [0.05–35]	0.81	0.79	(0.81)	1.94	0.61	1.02	0.34	0.66	0.31
KENN-J	Kennicutt [0.05–35]	0.90	0.76	(0.80)	1.94	0.64	1.00	0.32	0.66	0.31
LARS-A	Larson [0.01–100]	0.82	0.84	(0.86)	2.16	0.64	1.10	0.37	0.74	0.32
LARS-B	Larson [0.01–100]	0.94	0.78	(0.80)	2.16	0.69	1.06	0.34	0.74	0.32
LARS-C	Larson [0.01–22]	0.81	0.78	(0.84)	2.11	0.68	1.05	0.33	0.72	0.31
LARS-D	Larson [0.01–22]	0.83	0.79	(0.84)	2.11	0.67	1.05	0.33	0.72	0.31
LARS-E	Larson [0.01–23]	0.95	0.74	(0.79)	2.11	0.71	1.01	0.31	0.72	0.31
LMOD-B	mod. Larson [0.01–100]	0.74	0.93	(0.99)	2.18	0.59	1.18	0.40	0.75	0.31
LMOD-C	mod. Larson [0.01–100]	0.77	0.95	(1.01)	2.18	0.57	1.20	0.40	0.75	0.30
LMOD-D	mod. Larson [0.2–100]	0.86	0.82	(0.85)	1.96	0.60	1.05	0.35	0.75	0.28
LMOD-E	mod. Larson [0.2–100]	0.90	0.80	(0.84)	1.96	0.61	1.03	0.34	0.68	0.31
LMOD-F	mod. Larson [0.2–100]	0.93	0.80	(0.84)	1.96	0.61	1.03	0.34	0.68	0.31
CHAB-A	Chabrier [0.01–100]	0.78	0.95	(0.97)	2.54	0.67	1.27	0.41	0.87	0.32
CHAB-B	Chabrier [0.01–100]	0.88	0.91	(0.93)	2.54	0.70	1.24	0.39	0.87	0.32
CHAB-C	Chabrier [0.01–100]	0.95	0.88	(0.90)	2.54	0.72	1.21	0.38	0.87	0.31
CHAB-D	Chabrier [0.01–32]	0.83	0.94	(0.97)	2.53	0.67	1.26	0.40	0.87	0.31
CHAB-E	Chabrier [0.01–32]	0.87	0.91	(0.97)	2.53	0.70	1.23	0.38	0.87	0.31
CHAB-F	Chabrier [0.01–33]	0.92	0.90	(0.96)	2.53	0.70	1.23	0.38	0.87	0.31

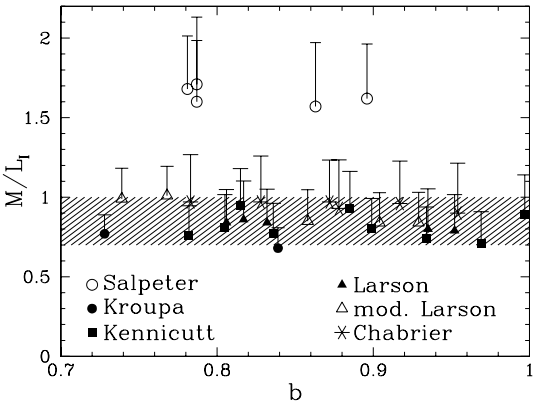

Figure 25. Estimated global M/L ratio of disc galaxies, including the contribution of the bulge. Dots represent the lower limit estimate (treating the bulge as an extension of the disc properties to the centre), bars indicate the upper limit estimate (treating the bulge as a 10 Gyr old SSP contributing 25 per cent of the total I-band luminosity). The shaded area marks the range $M/L_I = 0.7$–1 favoured by observations of Sbc–Sc spirals. This figure is available in colour in the on-line version of the journal on *Synergy*.

et al. 2003). We consider SSPs of age 10 Gyr, as characteristic of the bulges of early-type spirals (Peletier et al. 1999); this is likely to overestimate the M/L ratio of the bulges of Sbc/Sc galaxies, which tend to be younger (Carollo, Ferguson & Wyse 1999; Peletier et al. 1999). We consider SSPs of solar metallicity for simplicity. In the bulge of our galaxy, the bulk of stars is between half-solar and solar metallicity (McWilliam & Rich 1994; Zoccali et al. 2003) with a super-metal rich tail (Bertelli et al. 1995); varying the metallicity by a factor of 2 would change the bulge M/L ratio in the I band by 15 per cent or so, negligible for the sake of the rough estimates we are giving here. Column 5 of Table 6 lists the I-band M/L ratios of the stellar component (i.e. stars+remnants, excluding the re-ejected gas) of 10 Gyr old, solar SSPs with the same IMF as in the disc models.

Typically, the bulge-to-disc luminosity ratio in the I band, $(\mathcal{B}/\mathcal{D})_I$, is around 25 per cent for Sbc/Sc spirals, although with a large scatter (Sommer-Larsen et al. 2003). Assuming $(\mathcal{B}/\mathcal{D})_I = 0.25$ and the respective M/L ratios for disc and bulge, results in mass ratios between 50 and 70 per cent (column 6). This illustrates that the luminosity ratio, even in the red bands, is not a direct indicator of the mass ratio of the two components: allowance must be made for the different M/L ratio between an old bulge and the disc.

With the adopted value $(\mathcal{B}/\mathcal{D})_I = 25$ per cent and the respective M/L ratios, we estimate the global galactic M/L ratios in column 7 of Table 6. For the bottom-light IMFs, $M/L_I(\mathrm{tot}) = 1$–1.2 (see also Fig. 25). These values are strict upper limits, for two reasons. First, as mentioned above, bulges in Sbc/Sc spirals seem to be younger and/or host a younger component than the assumed 10 Gyr, so their characteristic M/L ratio is expected to be lower than in column 5. Secondly, here we are probably overestimating the luminosity contribution from the bulge: the typical value $(\mathcal{B}/\mathcal{D})_I \sim 0.25$ in Sommer-Larsen et al. (2003) is in fact derived from two-dimensional light decompositions assuming an $r^{1/4}$ profile for the bulge (Byun 1992). Nowadays, exponential light profiles or shallower Sérsic profiles are favoured for bulges, especially in late-type spirals (de Jong 1996a; Carollo et al. 1999, 2001; Balcells 2003); with an exponential profile, the decomposition yields significantly lower $\mathcal{B}/\mathcal{D}$ ratios (de Jong 1996a) and the bulge contribution to the total M/L ratio is correspondingly less. Note also that the global $(B-V)_0$ colours in Table 2, obtained for the global disc (extended to the centre) are in good agreement with the observed $(B-V) \sim 0.55$ of Sbc/Sc spirals (Roberts & Haynes 1994); hence the contribution of an old, red bulge cannot be very large.

In conclusion, since bulges in Sbc/Sc spirals seem to display, at odds with earlier types, a continuity of properties with the inner regions of discs (Carollo et al. 1999); the true global M/L ratio of an Sbc/Sc spiral should lie somewhere between the alternative values given in Table 6 and in Fig. 25.

8.1 M/L offsets with Hubble type: the bulge contribution

In this section we recompute the offsets in stellar M/L ratios – and correspondingly in the TF relation – as a function of Hubble type, discussed in Section 5.1, including the effect of bulges.

The b parameter we used as a Hubble-type indicator, is an indicator of the SFH in the disc (see Section 2), hence the offsets in stellar M/L ratios discussed in Section 5.1 are essentially due to the differences in disc properties. However, the bulge also contributes to the global M/L ratio, possibly in a different fashion in different Hubble types. It is not clear beforehand how the bulge contribution might change the disc-based offsets in Section 5.1. On one hand, the $\mathcal{B}/\mathcal{D}$ *luminosity* ratio increases toward earlier Hubble types; hence one might expect that bulges in earlier Hubble types are more prominent and contribute more to increasing the global M/L ratio of galaxies; this would enhance the systematic offset in M/L of earlier types with respect to Sbc/Sc. On the other hand, in earlier Hubble types the stellar populations in the disc per se are on average older and redder, so that the difference in M/L ratio between disc and bulge is less significant; hence one might expect that including the bulge has a lesser impact on the global M/L ratio for early types than for late types, reducing the net offsets.

In Table 7 we estimate the offsets in global M/L ratios as a function of Hubble type, adding the effect of the bulge to the simple disc models computed in Section 5. The M/L ratios for the discs (column 4) are taken from Section 5, those of the bulges (column 5) are derived from 10 Gyr old SSPs of solar metallicity. The $\mathcal{B}/\mathcal{D}$ ratios in the I band as a function of Hubble type (column 6) are from Sommer-Larsen et al. (2003). Computing the actual mass ratios (column 7) shows that the $\mathcal{B}/\mathcal{D}$ ratio in mass does not depend strongly on Hubble type, hence the trends in $\mathcal{B}/\mathcal{D}$ luminosity ratios are mostly due to different stellar populations and SFHs in the discs – as suggested by Kennicutt et al. (1994). For all Hubble types (and all IMFs) the typical $\mathcal{B}/\mathcal{D}$ mass ratio is around 60 per cent. However, we remind the reader that these estimates are derived considering the bulges of all Hubble types to be similar: 10 Gyr old red objects. As discussed above, this is a good estimate for Sa to Sb galaxies, less so for Sbc/Sc galaxies; if the latter have younger bulges, the mass $\mathcal{B}/\mathcal{D}$ ratio may still have a real trend with Hubble type. Besides, what we are discussing here are gross average trends, but the scatter in $\mathcal{B}/\mathcal{D}$ ratios is known to be large (de Jong 1996a; Sommer-Larsen et al. 2003 and references therein). In particular, bulgeless disc galaxies are also observed, especially among late Hubble types.

Including the effect of the bulge, the typical stellar M/L ratio is $\sim$1.5 times larger in Sa/Sab galaxies than in Sbc/Sc galaxies (column 9). The corresponding systematic offsets in magnitude with respect to the Sbc/Sc zero-point are approximately 0.25–0.3 mag for Sb galaxies and 0.4–0.5 mag for Sa/Sab (column 10). In summary, the effect of the bulge is to *reduce* the offsets expected from the sole

Table 7. Total M/L ratios, M/L and magnitude offsets as a function of Hubble type, including the contribution of the bulge. (1) Hubble type. (2) Typical b parameter for the disc. (3) Adopted IMF (mass limits as in Section 3). (4) M/L ratio in the I band for the disc, from the simple models in Section 5. (5) M/L ratio in the I band for the bulge, considered as an SSP of solar metallicity and age 10 Gyr. (6) $\mathcal{B}/\mathcal{D}$ luminosity ratio in the I band. (7) Actual $\mathcal{B}/\mathcal{D}$ mass ratio. (8) Global M/L ratio in the I band for the galaxy. (9) Offset in M/L ratio with respect to Sbc/Sc galaxies. (10) Offset in magnitude with respect to Sbc/Sc galaxies. (11) M/L ratio in the K band for the disc (from the simple models in Section 5). (12) M/L ratio in the K band for the bulge (considered as an SSP of solar metallicity and age 10 Gyr). (13) $\mathcal{B}/\mathcal{D}$ luminosity ratio in the K band corresponding to the mass ratio in column 7, or equivalently to the adopted $(\mathcal{B}/\mathcal{D})_I$ in column 6.

(1) Hubble type	(2) b	(3) IMF	(4) $\frac{M_*}{L_I}(\mathcal{D})$	(5) $\frac{M_*}{L_I}(\mathcal{B})$	(6) $\left(\frac{\mathcal{B}}{\mathcal{D}}\right)_I$	(7) $\frac{M_*(\mathcal{B})}{M_*(\mathcal{D})}$	(8) $\frac{M_*}{L_I}$(tot)	(9) $\Delta(\frac{M_*}{L_I})$	(10) $\Delta\,(m_I)$	(11) $\frac{M_*}{L_K}(\mathcal{D})$	(12) $\frac{M_*}{L_K}(\mathcal{B})$	(13) $\left(\frac{\mathcal{B}}{\mathcal{D}}\right)_K$
Sa/Sab	0.1	Salpeter	2.70	3.77	0.45	0.63	3.03	1.54	0.47	0.99	1.31	0.48
Sb	0.35	Salpeter	2.09	3.77	0.35	0.63	2.53	1.28	0.27	0.80	1.31	0.38
Sbc/Sc	0.9	Salpeter	1.52	3.77	0.25	0.62	1.97	1	0	0.61	1.31	0.29
Sa/Sab	0.1	Kroupa	1.76	2.35	0.45	0.60	1.94	1.43	0.39	0.64	0.82	0.47
Sb	0.35	Kroupa	1.44	2.35	0.35	0.57	1.68	1.23	0.23	0.55	0.82	0.38
Sbc/Sc	0.9	Kroupa	1.11	2.35	0.25	0.53	1.36	1	0	0.45	0.82	0.29
Sa/Sab	0.1	Kennicutt	1.29	1.80	0.45	0.63	1.45	1.41	0.37	0.47	0.61	0.48
Sb	0.35	Kennicutt	1.02	1.80	0.35	0.62	1.22	1.26	0.25	0.39	0.61	0.39
Sbc/Sc	0.9	Kennicutt	0.76	1.80	0.25	0.59	0.97	1	0	0.31	0.61	0.30
Sa/Sab	0.1	Larson(1)	1.52	2.16	0.45	0.64	1.72	1.62	0.52	0.55	0.74	0.48
Sb	0.35	Larson(1)	1.13	2.16	0.35	0.67	1.40	1.31	0.29	0.43	0.74	0.39
Sbc/Sc	0.9	Larson(1)	0.79	2.16	0.25	0.69	1.06	1	0	0.32	0.74	0.29
Sa/Sab	0.1	Larson(2)	1.56	2.18	0.45	0.63	1.75	1.50	0.44	0.57	0.75	0.47
Sb	0.35	Larson(2)	1.22	2.18	0.35	0.62	1.47	1.26	0.25	0.47	0.75	0.38
Sbc/Sc	0.9	Larson(2)	0.91	2.18	0.25	0.60	1.17	1	0	0.37	0.75	0.29
Sa/Sab	0.1	Chabrier	1.72	2.54	0.45	0.67	1.97	1.59	0.51	0.62	0.87	0.48
Sb	0.35	Chabrier	1.29	2.54	0.35	0.69	1.61	1.30	0.29	0.49	0.87	0.39
Sbc/Sc	0.9	Chabrier	0.91	2.54	0.25	0.70	1.24	1	0	0.36	0.87	0.29

differences in disc SFH (Section 5). The offsets, however, remain significant.

The present estimate is a lower limit to the expected offsets, since the effect of bulges is maximized. As discussed in Section 8, the I-band $\mathcal{B}/\mathcal{D}$ ratios from Sommer-Larsen et al. (2003) are likely to be overestimated, because they are derived from a decomposition performed with an $r^{1/4}$ profile, hence in Table 7 we are overestimating the effects of bulges. In addition, if bulges in Sbc/Sc galaxies are younger, the global M/L ratios of these galaxies are lower than listed in Table 7, and the difference with respect to earlier types becomes more significant. All in all, the typical magnitude offsets should lie between the values in Table 7 and the estimates given in Section 5 from the pure disc contributions.

8.2 The bulge-to-disc ratio in the *K* band

It is very common nowadays to assess issues such as the stellar mass distribution in galaxies and the $\mathcal{B}/\mathcal{D}$ ratio from observations in NIR bands (supposedly better mass tracers than blue or optical bands, since an important contribution to the light in NIR bands comes from the underlying old stellar component). We stressed in Section 5.2 the uncertainties in estimating *absolute* M/L ratios in NIR bands, especially due to the role of AGB stars, a complex phase with uncertain modelling in population synthesis. However, as an estimate of *relative* mass content, NIR bands are still useful. For instance, in Fig. 8 different treatments of the AGB phase (G-SSPs versus M-SSPs) seem to result in overall offsets of the K-band M/L ratios, while the trend as a function of the b parameter is preserved. Therefore, comparing the NIR luminosity of two objects, we still get an indication of their stellar mass content in relative terms, while deriving their absolute stellar mass from the M/L ratio would be more model-dependent.

Since a lot of focus is set nowadays on NIR observations and surveys (e.g. 2MASS, DENIS), it is useful to present the $\mathcal{B}/\mathcal{D}$ ratios we predict in the K band, and discuss to what extent the K-band luminosity can be considered a direct tracer of stellar mass.

In Table 6, we list the K-band M/L ratios for our model Sbc/Sc discs (column 8) and for the bulges, modelled as 10 Gyr old SSPs of solar metallicity (column 9). We verified that changing the typical metallicity of the bulge by a factor of 2 with respect to solar, would change the bulge M/L_K ratio by less than 10 per cent. In column 10 we list the resulting $\mathcal{B}/\mathcal{D}$ ratios in the K band when the mass ratios from column 6 are assumed; these are the $(\mathcal{B}/\mathcal{D})_K$ ratios corresponding to the adopted value $(\mathcal{B}/\mathcal{D})_I = 25$ per cent in the I band, for Sbc/Sc galaxies. In all cases, the typical value $(\mathcal{B}/\mathcal{D})_K = 30$ per cent, which is in good agreement, within the large scatter, with the findings of de Jong (1996a) for Sbc/Sc galaxies in his $r^{1/4}$ bulge–disc decompositions in the K band. Still, the K-band $\mathcal{B}/\mathcal{D}$ ratio is not a direct indicator of the corresponding mass ratio, due to the typical differences in stellar populations and M/L ratio between bulge and disc (cf. column 10 versus column 6).

In Table 7, columns 11–13, we list the K-band M/L ratios for discs of different Hubble type (from the simple models in Section 5), the M/L ratios of bulges, and the K-band $\mathcal{B}/\mathcal{D}$ ratios corresponding to the mass ratios in column 7, i.e. corresponding to the $(\mathcal{B}/\mathcal{D})_I$ ratios adopted in column 6. The typical $\mathcal{B}/\mathcal{D}$ ratio in the K band is 30 per cent for late-type spirals, 40 per cent for Sb spirals and 50 per cent for early-type Sa/Sab spirals. These values and trends with Hubble type are in excellent agreement with de Jong (1996a) for his $r^{1/4}$ bulge–disc decompositions; however, we are speaking of average

trends but the observational scatter is huge (de Jong 1996a). For no Hubble type can the K-band $\mathcal{B}/\mathcal{D}$ ratio be considered a direct indicator of the corresponding mass ratio (cf. column 13 versus column 7), so that to derive the $\mathcal{B}/\mathcal{D}$ mass ratio one should always account for the different stellar populations and M/L ratios between bulge and disc.

9 SUMMARY AND CONCLUSIONS

In the introduction we reviewed some theoretical and observational evidence that the M/L ratio of the stellar component in late-type spirals should be low: $M/L_I < 1$ in the I band. This paper is devoted to discussing whether M/L ratios that are so low are compatible with the current understanding of stellar populations in galaxies. We explained in Section 2 why we should concentrate on late-type spirals such as Sbc/Sc, characterized by a SFH with 'birth rate parameter' $b \geqslant 0.8$, and we argued that the I band is the optimal band for estimates of M/L ratios. In this study we considered the 'classic' Salpeter IMF, mostly for the sake of comparison, and other more 'bottom-light' IMFs favoured by independent studies: the Kroupa IMF, the Kennicutt IMF, the Larson IMF (also in a modified version) and the Chabrier IMF (Section 3). We calculated up-to-date sets of SSPs for a wide range of metallicities with these different IMFs, to compute the corresponding galactic photometry (Section 4). A simple approach, based on one-zone models with exponential SFHs and fixed metallicity, was presented in Section 5 showing that, aside from the Salpeter IMF which has a high M/L ratio, all the other IMFs imply $M/L_I \leqslant 1$ for Sbc/Sc galaxies. Our models also predict a significant difference in typical M/L ratios – and hence in the zero-point of the TF-relation – between spirals of different Hubble type. We used our simple models to show that the predicted M/L ratio in the I band is quite robust with respect to uncertainties in the current SSPs (mostly the contribution of the AGB phase), in contrast to NIR bands. Furthermore, we assessed uncertainties related to spectral libraries. We estimated our M/L ratios to be robust to within 10 per cent or better for the typical metallicities of spiral galaxies, and to be conservatively high.

For a more realistic analysis, we developed chemo-photometric models with gas infall and radial gradients in SFH and metallicity, to discuss M/L ratios in connection with the chemical properties of spiral discs of Sbc/Sc type. Overall the M/L ratios from full chemo-photometric models agree quite well with the predictions of simple exponential models, but some further insight is obtained when considering the corresponding chemical evolution.

As a result of the low locked-up fractions, some of the bottom-light IMFs (Kennicutt, Larson and Chabrier) result in high metal yields, which are hardly compatible with the observed metallicities and gas fractions – unless metallicities are heavily underestimated due to dust depletion, but this seems unlikely (Section 7.5). Either we reduce the typical metal production (by means of suitable tuning of the upper mass limits of the IMF, or by allowing for fallback of metals on to a black hole after the SN explosion), or we need to invoke dispersal of metals from disc galaxies into the intergalactic medium, a behaviour reminiscent of cluster galaxies enriching the intracluster medium. In any case, the resulting M/L ratio for Sbc/Sc discs is $M/L_I \sim 0.7$–0.9.

In other cases (Kroupa and modified-Larson IMFs), the slope of the IMF at high masses is quite steep and the metal production turns out to be low; then the net yield must be increased to obtain Sbc/Sc discs with the observed metallicities. This is accomplished by tuning the lower-mass end to larger values, thereby decreasing the locked-up fraction but also, correspondingly, the M/L ratio. Also in this case, we find $M/L_I \sim 0.8$ for Sbc–Sc discs.

Although uncertainties in the gas fractions (a basic constraint for chemical evolution models) and in the theoretical stellar yields may hamper the quantitative details of the models, e.g. the exact tuning on the IMF mass limits, the predicted M/L ratios appear to be rather robust with respect to these details. We consistently find that low M/L ratios, $M/L_I \sim 0.8$ for the typical SFHs of Sbc/Sc discs, naturally follow from currently popular, 'bottom-light' models of the stellar IMF. Even after including the contribution of bulges to the overall M/L ratio of disc galaxies, we globally find a typical $M/L_I \lesssim 1$ with the 'bottom-light' IMFs.

ACKNOWLEDGMENTS

We are grateful to Léo Girardi for many clarifications on stellar isochrones and photometry. We also benefited from suggestions and comments by P. Salucci, R. Kennicutt, A. Bressan, S. Yi, S. Courteau, J. Mould, A. Weiss, L. Piovan and B. Gibson. We thank our anonymous referee for very useful remarks. LP acknowledges kind hospitality from the Astronomy Department of Padua University and from the Observatory of Helsinki on various visits. This study has been financed by the Danmarks Grundforskningsfond, through the funding of TAC, and by the Italian MIUR.

REFERENCES

Aaronson M., Bothun G., Mould J., Huchra J., Schommer R.A., Cornell M.E., 1986, ApJ, 302, 536
Abadi M.G., Navarro J.F., Steinmetz M., Eke V.R., 2003, ApJ, 591, 499
Balcells M., 2003, in Boily C. M., Patsis P., Portegies Zwart S., Spurzem R., Theis C., eds, Proc. JENAM 2002, Galactic and Stellar Dynamics. EAS Publication Series, Vol. 10, p. 23
Bell E.F., de Jong R.S., 2000, MNRAS, 312, 497
Bell E.F., de Jong R.S., 2001, ApJ, 550, 212 (BdJ)
Benson A.J., Bower R.G., Frenk C.S., White S.D.M., 2000, MNRAS, 314, 557
Bertelli G., Bressan A., Chiosi C., Ng Y.K., Ortolani S., 1995, A&A, 301, 381
Bettoni D., Galletta G., García-Burillo S., 2003, A&A, 405, 5
Binney J., Merrifield M., 1998, Galactic Astronomy. Princeton Univ. Press, Princeton
Boissier S., Prantzos N., 1999, MNRAS, 307, 857
Boselli A., Lequeux J., Gavazzi G., 2002, A&A, 384, 33
Bottema R., 1993, A&A, 275, 16
Bottema R., 1997, A&A, 328, 517
Bottema R., 2002, A&A, 388, 809
Bregman J.N., 1980, ApJ, 236, 577
Bressan A., Chiosi C., Fagotto F., 1994, ApJS, 94, 63
Bressan A., Granato G., Silva L., 1998, A&A, 332, 135
Bruzual G., 1983, ApJ, 273, 105
Bruzual G., Charlot S., 1993, ApJ, 405, 538
Buchhorn M., 1992, PhD thesis, Australian National Univ., Canberra
Burkert A., Truran J.W., Hensler G., 1992, ApJ, 391, 651
Buzzoni A., 1999, in Sato K., ed., Proc. IAU Symp. 183, Cosmological Parameters and the Evolution of the Universe. Kluwer, Dordrecht, p. 134
Buzzoni A., 2002, in Chavez M., Bressan A., Buzzoni A., Mayya D., eds, New Quests in Stellar Astrophysics: the Link between Stars and Cosmology. Kluwer ASSL, Vol. 274. Kluwer, Dordrecht (astro-ph/0107273)
Byun Y.-I., 1992, PhD thesis, Australian National Univ., Canberra

Carraro G., 2000, in Matteucci F., Giovannelli F., eds, The Evolution of the Milky Way: Stars versus Clusters. Kluwer ASSL, Vol. 255. Kluwer, Dordrecht, p. 335
Carollo C.M., Ferguson H.C., Wyse R.F.G., 1999, The Formation of Galactic Bulges. Cambridge Univ. Press, Cambridge
Carollo C.M., Stiavelli M., de Zeeuw P.T., Seigar M., Dejonghe H., 2001, ApJ, 546, 216
Castelli F., Gratton R.G., Kurucz R.L., 1997, A&A, 318, 841
Chabrier G., 1999, ApJ, 513, L103
Chabrier G., 2001, ApJ, 554, 1274
Chabrier G., 2002, ApJ, 567, 304
Chabrier G., 2003, PASP, 115, 763
Chiappini C., Matteucci F., Gratton R.G., 1997, ApJ, 477, 765
Chiosi C., 2000, A&A, 364, 423
Chiosi C., Bertelli G., Bressan A., 1992, ARA&A, 30, 235
Chiosi C., Bressan A., Portinari L., Tantalo R., 1998, A&A, 339, 355
Colpi M., Shapiro S.L., Wasserman I., 1996, ApJ, 470, 1075
Courteau S., 1997, AJ, 114, 2402
Courteau S., Rix H.W., 1999, ApJ, 513, 561
Courteau S., Willick J.A., Strauss M.A., Schlegel D., Postman M., 2000, ApJ, 544, 636
Dale D.A., Giovanelli R., Haynes M.P., Campusano L.E., Hardy E., 1999, AJ, 118, 1489
Dame T.M., 1993, in Holt S.S., Verter F., eds, Proc. AIP Conf. 278, Back to the Galaxy. AIP, New York, p. 267
de Blok W.J.G., Bosma A., 2002, A&A, 385, 816
de Blok W.J.G., McGaugh S.S., Rubin V.C., 2001a, AJ, 122, 2396
de Blok W.J.G., McGaugh S.S., Bosma A., Rubin V.C., 2001b, ApJ, 552, L23
de Jong R.S., 1996a, A&A, 313, 45
de Jong R.S., 1996b, A&A, 313, 377
de Jong R.S., Bell E.F., 2001, in Funes J.G., S.J., Corsini E.M., eds, ASP Conf. Ser. Vol. 230, Galaxy Disks and Disk Galaxies. Astron. Soc. Pac., San Francisco, p. 555
de Mello D.F., Maia M.A.G., Wiklind T., 2002a, A&A, 381, 761
de Mello D.F., Wiklind T., Maia M.A.G., 2002b, A&A, 381, 771
Dehnen W., Binney J.J., 1998, MNRAS, 294, 429
Dopita M.A., Ryder S.D., 1994, ApJ, 430, 163
Dwek E., 1998, ApJ, 501, 643
Efstathiou G., Lake G., Negroponte J., 1982, MNRAS, 199, 1069
Eke V., Navarro J.F., Steinmetz M., 2001, ApJ, 554, 114
Finoguenov A., Burkert A., Böhringer H., 2003, ApJ, 594, 136
Fraternali F., Oosterloo T., Sancisi R., van Moorsel G., 2001, ApJ, 562, L47
Freeman K., 1970, ApJ, 160, 811
Fuchs B., 2002, in Klapdour-Kleingrothaus H.V., Viollier R., eds, Dark Matter in Astro and Particle Physics. Springer-Verlag, Berlin, p. 28
Fuchs B., 2003a, Ap&SS, 284, 719
Fuchs B., 2003b, in Spooner N.J.C., Kudryavtsev V., eds, Proc. 4th International Workshop on the Identification of Dark Matter. Singapore, World Scientific, p. 72
Garnett D., Shields G., Skillman E., Sagan S., Dufour R., 1997, ApJ, 489, 63
Gerhard O., 2002, Space Sci. Rev., 100, 129
Giovanelli R., Haynes M.P., Salzer J.J., Wegner G., da Costa L.N., Freudling W., 1995, AJ, 110, 1059
Giovanelli R., Haynes M.P., Herter T., Vogt N.P., 1997a, AJ, 113, 53
Giovanelli R., Haynes M.P., Herter T., Vogt N.P., 1997b, ApJ, 477, L1
Girardi L., Bertelli G., 1998, MNRAS, 300, 533
Girardi L., Bressan A., Bertelli G., Chiosi C., 2000, A&AS, 141, 371
Girardi L., Bressan A., Bertelli G., Chiosi C., Groenewegen M.A.T., Marigo P., Salasnich B., Weiss A., 2002, A&A, 391, 195
Gould A., Bahcall J.N., Flynn C., 1997, ApJ, 482, 913
Gould A., Flynn C., Bahcall J.N., 1998, ApJ, 503, 798
Gratton R.G., Carretta E., Matteucci F., Sneden C., 2000, A&A, 358, 671
Guiderdoni B., Rocca-Volmerange B., 1987, A&A, 186, 1
Gummersbach C.A., Kaufer A., Schäfer D.R., Szeifert T., Wolf B., 1998, A&A, 338, 881
Han M., Mould J.R., 1992, ApJ, 396, 453
Heckman T.M., 2002, in Mulchaey J.S., Stocke J., eds, ASP Conf. Ser. Vol. 254, Extragalactic Gas at Low Redshift. Astron. Soc. Pac., San Francisco, p. 292
Iben I., Jr, 1991, ApJS, 76, 55
Kannappan S.J., Fabricant D.G., Franx M., 2002, AJ, 123, 2358
Kennicutt R.C., 1983, ApJ, 272, 54
Kennicutt R.C., Tamblyn P., Congdon C.W., 1994, ApJ, 435, 22 (KTC94)
Kent S.M., 1987, AJ, 93, 816
Kent S.M., Dame T.M., Fazio G., 1991, ApJ, 378, 131
Kranz T., Slyz A., Rix H.-W., 2003, ApJ, 586, 143
Kroupa P., 1998, in Rebolo R., Martin E.L., Zapatero Osorio M.R., eds, ASP Conf. Ser. Vol. 134, Brown Dwarfs and Extrasolar Planets. Astron. Soc. Pac., San Francisco, p. 483
Kroupa P., 2001, MNRAS, 322, 231
Kroupa P., 2002, Sci, 295, 82
Kroupa P., Tout C.A., Gilmore G., 1993, MNRAS, 262, 545
Larson R.B., 1976, MNRAS, 176, 31
Larson R.B., 1986, MNRAS, 218, 409
Larson R.B., 1998, MNRAS, 301, 569
Larson R.B., Tinsley B.M., 1978, ApJ, 216, 46
Lejeune T., Cuisinier F., Buser R., 1997, A&AS, 125, 229
Lejeune T., Cuisinier F., Buser R., 1998, A&AS, 130, 65
Liu M.C., Charlot S., Graham J.R., 2000, ApJ, 543, 644
Lynden-Bell D., 1975, Vistas Astron., 19, 229
MacFadyen A.I., Woosley S.E., Heger A., 2001, ApJ, 550, 410
McGaugh S., 2001, in Funes J.G., S.J., Corsini E.M., eds, ASP Conf. Ser. Vol. 230, Galaxy Disks and Disk Galaxies. Astron. Soc. Pac., San Francisco, p. 541
McGaugh S., 2003, in Bender R., Renzini A., eds, Proc. ESO Workshop, The Mass of Galaxies at Low and High Redshift. ESO, Garching, p. 45
McGaugh S., Schombert J.M., Bothun G.D., de Blok W.J.G., 2000, ApJ, 533, L99
McWilliam A., Rich M., 1994, ApJS, 91, 749
Macri L.M., Huchra J., Sakai S., Mould J.R., Hughes S.M.G., 2000, ApJS, 128, 461
Marchesini D., D'Onghia E., Chincarini G., Firmani C., Conconi P., Molinari E., Zacchei A., 2002, ApJ, 575, 801
Marigo P., 2001, A&A, 370, 194
Marigo P., 2002, A&A, 387, 507
Marigo P., Girardi L., 2001, A&A, 377, 132
Marigo P., Girardi L., Chiosi C., 2003, A&A, 403, 225
Masset F.S., Bureau M., 2003, ApJ, 586, 152
Mathewson D.S., Ford V.L., Buchhorn M., 1992, ApJS, 81, 413
Matteucci F., François P., 1989, MNRAS, 239, 885
Miller G.E., Scalo J.M., 1979, ApJ, 41, 513
Möller C., Fritze-v. Alvensleben U., Fricke K.J., 1997, A&A, 317, 676
Moretti A., Portinari L., Chiosi C., 2003, A&A, 408, 431
Mouhcine M., 2002, A&A, 394, 125
Mouhcine M., Lançon A., 2002, A&A, 393, 149
Mould J. et al., 2000, ApJ, 528, 655
Navarro J.F., Steinmetz M., 2000a, ApJ, 528, 607
Navarro J.F., Steinmetz M., 2000b, ApJ, 538, 477
Navarro J.F., Frenk C.S., White S.D.M., 1995, MNRAS, 275, 56
Ng Y.K., Bertelli G., Bressan A., Chiosi C., Lub J., 1995, A&A, 295, 655
Ostriker J.P., Peebles P.J.E., 1973, ApJ, 186, 467
Padoan P., Nordlund Å, A&A, 2002, ApJ, 576, 870
Pagel B.E.J., 1997, Nucleosynthesis and Chemical Evolution of Galaxies. Cambridge Univ. Press, Cambridge
Pagel B.E.J., 2002, in Fusco-Femiano R., Matteucci F., eds, ASP Conf. Ser. Vol. 253, Chemical Enrichment of Intracluster and Intergalactic Medium. Astron. Soc. Pac., San Francisco, p. 489

Peletier R.F., Balcells M., Davies R.L., Andredakis Y., Vazdekis A., Burkert A., Prada F., 1999, MNRAS, 310, 703
Pettini M., Steidel C.C., Adelberger K.L., Dickinson M., Giavalisco M., 2000, ApJ, 528, 96
Piotto G., Zoccali M., 1999, A&A, 345, 485
Piovan L., Tantalo R., Chiosi C., 2003, A&A, 408, 559
Podsiadlowski P., Nomoto K., Maeda K., Nakamura T., Mazzali P., Schmidt B., 2002, ApJ, 567, 491
Portinari L., Chiosi C., 1999, A&A, 350, 827
Portinari L., Chiosi C., Bressan A., 1998, A&A, 334, 505
Prantzos N., Boissier S., 2000, MNRAS, 313, 338
Ratnam C., Salucci P., 2000, New Astron., 5, 427
Reid I.N., Gizis J.E., 1997, AJ, 113, 2246
Renzini A., Buzzoni A., 1986, in Chiosi C., Renzini A., eds, Spectral Evolution of Galaxies. Reidel, Dordrecht, p. 195
Roberts M.S., Haynes M.P., 1994, ARA&A, 32, 115
Rubin V.C., Burstein D., Ford W.K., Thonnard N., 1985, ApJ, 289, 81
Sackett P.D., 1997, ApJ, 483, 103
Sakai S. et al., 2000, ApJ, 529, 698
Salaris M., Chieffi A., Straniero O., 1993, ApJ, 414, 580
Salasnich B., Girardi L., Weiss A., Chiosi C., 2000, A&A, 361, 1023
Salpeter E.E., 1955, ApJ, 121, 161
Salucci P., 2001, MNRAS, 320, L1
Salucci P., Borriello A., 2001, MNRAS, 323, 285
Scalo J.M., 1986, Fund. Cosmic Phys., 11, 1
Schechter P.L., 1980, AJ, 85, 801
Schmidt M., 1959, ApJ, 129, 243
Schulz J., Fritze-v. Alvensleben U., Möller C.S., Fricke K.J., 2002, A&A, 392, 1
Silk J., 2003, MNRAS, 343, 249
Simien F., de Vaucouleurs G., 1986, ApJ, 302, 564
Smartt S.J., Rolleston W.R.J., 1997, ApJ, 481, L47
Sommer-Larsen J., 1991, MNRAS, 250, 356
Sommer-Larsen J., 1996, ApJ, 457, 118
Sommer-Larsen J., Dolgov A., 2001, ApJ, 551, 608
Sommer-Larsen J., Gelato S., Vedel H., 1999, ApJ, 519, 501
Sommer-Larsen J., Götz M., Portinari L., 2003, ApJ, 596, 47
Tantalo R., Chiosi C., Bressan A., Fagotto F., 1996, A&A, 311, 361
Thacker R.J., Couchman H.M.P., 2001, ApJ, 555, L17
Thomas D., Greggio L., Bender R., 1998, MNRAS, 296, 119
Tinsley B.M., 1980, Fund. Cosmic Phys., 5, 287
Trott C.M., Webster R.L., 2002, MNRAS, 334, 621
Tsujimoto T., Yoshii Y., Nomoto K., Matteucci F., Thielemann F.K., Hashimoto M., 1997, ApJ, 483, 228 (T97)
Tully R., 1988, Nat, 334, 209
Tully R., Fouqué P., 1985, ApJS, 58, 67
Tully R., Pierce M.J., Huang J.-S., Saunders W., Verheijen M.A.W., Witchalls P.L., 1998, AJ, 115, 2264
Vallejo O., Braine J., Baudry A., 2002, A&A, 387, 429
van Loon J.T. et al., 2003, MNRAS, 338, 857
van Zee L., Salzer J.J., Haynes M.P., O'Donoghue A.A., Balonek T.J., 1998, AJ, 116, 2805
Vazdekis A., Casuso E., Peletier R.F., Beckman J.E., 1996, ApJS, 106, 307
Vazdekis A., Peletier R.F., Beckman J.E., Casuso E., 1997, ApJS, 111, 203
Westera P., Lejeune T., Buser R., Cuisinier F., Bruzual G., 2002, A&A, 381, 524
Willick J., 1990, ApJ, 351, L5
Willick J., 1991, PhD thesis, Univ. California, Berkeley
Willick J., Courteau S., Faber S.M., Burstein D., Dekel A., 1995, ApJ, 446, 12
Willick J., Courteau S., Faber S.M., Burstein D., Dekel A., Kolatt T., 1996, ApJ, 457, 460
Young J.S., Knezek P.M., 1989, ApJ, 347, L55
Zampieri L., Shapiro S.L., Colpi M., 1998, ApJ, 502, L149
Zoccali M., Cassisi S., Frogel J.A., Gould A., Ortolani S., Renzini A., Rich R.M., Stephens A.W., 2000, ApJ, 530, 418
Zoccali M. et al., 2003, A&A, 399, 931

APPENDIX A: THE ZERO-POINT OF THE *I*-BAND TF RELATION

One of the motivations for this study was the need for a low M/L ratio in galactic discs to match the observed TF relation (Section 1). However, there are differences in the zero-point of the TF relation among different samples.

In Fig. A1 we compare different *I*-band TF relations based on large samples of cluster and/or field galaxies, as rescaled by their authors to the respective kinematic zero-points. The TF relation by Giovanelli et al. is based on a sample of 24 clusters, and the zero-point is set by requiring that the galaxies in the 14 most distant ones move on average with the Hubble flow (negligible peculiar velocities). A better kinematic zero-point, based on a sample of 52 distant clusters, has been determined by Dale et al. (1999), making the TF relation 0.1 mag dimmer than that by Giovanelli et al. Still, even with this correction there is a mismatch with other samples (see Fig. A1, top panel).

The sample by Han & Mould (1992, and companion papers) as reanalysed in the MARK III catalogue by Willick et al. (1995), is also a large deep sample of 24 clusters, with the zero-point set by requiring that the global sample is on average moving as a pure Hubble flow. The sample by Mathewson, Ford & Buchhorn (1992), also reanalysed in the MARK III catalogue, is a large sample of

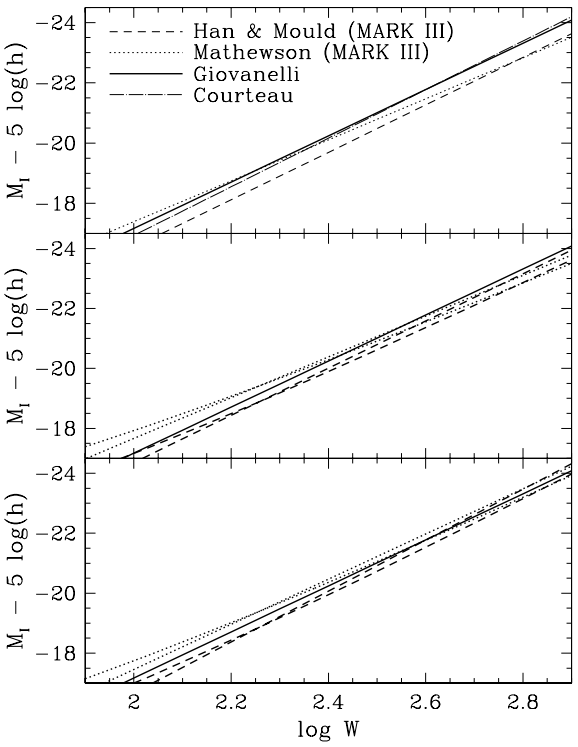

Figure A1. Comparison of different *I*-band TF relations with kinematic zero-points, from Giovanelli et al. (1997b), from the MARK III catalogue (Willick et al. 1995, 1996) and from Courteau et al. (2000). Middle panel, relations rescaled to a common W_{50} (see the text). Bottom panel, inverse MARK III TF relations, rescaled to W_{50} (see the text). This figure is available in colour in the on-line version of the journal on *Synergy*.

relatively nearby, mostly field spirals, normalized to the Han & Mould sample in linewidths and kinematic zero-point (Willick et al. 1996); compared with the other two TF relations, this is more influenced by peculiar motions and bulk flows due to the vicinity of the galaxies. The TF relation by Giovanelli et al., which we used as a reference in Fig. 1, is the brightest. The large offset between the sample by Giovanelli et al. and that by Han & Mould can be explained partly by the different definitions of linewidth used: at 50 and 20 per cent of the maximum H I flux, respectively (W_{50} and W_{20}; Willick 1990; Han & Mould 1992). The two estimates can differ by up to 10 per cent (Aaronson et al. 1986; Macri et al. 2000; Sakai et al. 2000) or 0.04 in logarithm. Since the TF relation is so steep, minor systematic offsets in the estimate of the circular velocity become crucial for the zero-point in luminosity.

These offsets in velocity widths are unimportant when the TF relation is used as a relative distance indicator or to map the peculiar velocity field (provided the definition is consistent within the sample), but they correspond to large effects in luminosity when the TF relation is used to test galactic models. The question obviously arises as to which TF relation should galactic models be compared with. In Sommer-Larsen & Dolgov (2001) and Sommer-Larsen et al. (2003) the circular velocity of the simulated disc galaxies is defined as the circular velocity at $R = 2.2\ R_{\rm d}$. For Milky Way sized galaxies this corresponds quite well to the maximum circular velocity, as obtained from optical rotation curves (Courteau 1997; Sackett 1997). As to radio linewidths, W_{50} is the one that best matches twice the optical maximum velocity (Buchhorn 1992; Mathewson et al. 1992; Courteau 1997), and it is used in the sample of Giovanelli et al. – with some further corrections to recover the true maximum rotational velocity (Giovanelli et al. 1997a). In the middle panel of Fig. A1 we rescale the two TF relations of the MARK III samples from W_{20} to W_{50}, dividing by 0.91 (Macri et al. 2000) or applying the corrections by Willick (1991), as in Han & Mould (1992). These samples are now closer in zero-point to the Giovanelli sample, yet with different conversions the difference in zero-point can reach 0.4 mag for Milky Way sized galaxies (log W ~ 2.6), with the TF of Giovanelli et al. being the brightest for $V_{\rm c} \gtrsim$ 130 km s^{-1}.

Other effects may contribute to these magnitude offsets, most notably different internal dust corrections (Giovanelli et al. 1995 versus Willick et al. 1996) or a different mixture of Hubble types. The TF relation of Giovanelli et al. has been corrected to apply to late-type spirals, while the other relations are averaged over Hubble type. All samples consist mostly of galaxies between Sb and Sc, but the systematic offset in magnitude of Sb galaxies may be larger than estimated by Giovanelli et al. (see our model predictions in Sections 5.1 and 8.1).

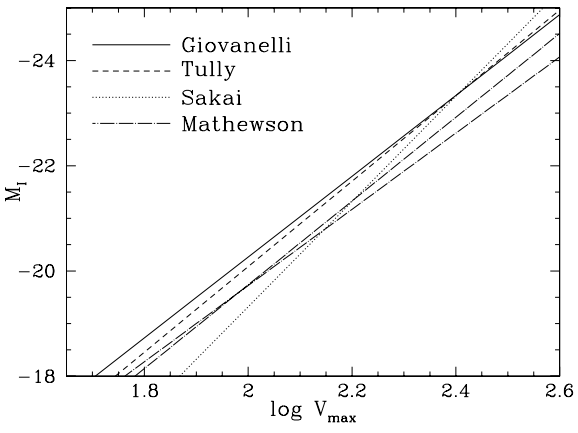

Figure A2. Comparison of different *I*-band TF relations with locally calibrated zero-points; from Giovanelli et al. (1997b), Tully et al. (1998), Sakai et al. (2000), Mathewson et al. (1992) and Buchhorn (1992). This figure is available in colour in the on-line version of the journal on *Synergy*.

On the other hand, the TF relation of Giovanelli et al. agrees well with that by Courteau et al. (2000), based on ∼300 galaxies at a distance of approximately 6000 km s^{-1} (shown only in the top panel of Fig. A1 for the sake of clarity).

Fig. A2 compares available *I*-band TF relations in absolute magnitude, calibrated using galaxies with Cepheid-based, absolute distances. All relations are expressed as a function of the maximum rotational velocity $V_{\rm max}$.

Here the TF relation of Giovanelli et al. is plotted according to their calibration using a local sample with known Cepheid distances, corresponding to $h = 0.69$ (Giovanelli et al. 1997b), hence very close to the relation plotted in Fig. 1 where $h = 0.65$ was used. Their linewidths W_{50} are corrected so as to give directly a good estimate of twice $V_{\rm max}$ (Giovanelli et al. 1997a).

The relation of Tully et al. (1998) is based on two clusters (Ursa Major and Pisces) and calibrated with local galaxies of known Cepheid distances. To convert their linewidth W_R to $V_{\rm max}$ we adopted the corrections by Tully & Fouqué (1985).

The TF relation of Sakai et al. (2000) is based on a combination of a local sample (with Cepheid distances obtained from the *Hubble Space Telescope* H_0 Key Project) and the sample by Giovanelli et al. We assume here that the linewidth they use, W_{50}, corresponds well to twice $V_{\rm max}$ – see above.

The Mathewson TF relations are those defined by Mathewson et al. (1992) for Fornax, and by Buchhorn (1992) combining clusters and groups in the Mathewson sample (hence these TF relations differ from the global Mathewson/MARK III TF in Fig. A1). We rescaled both relations to the recent, Cepheid-based estimates of the Fornax distance modulus, 31.5 on average (Mould et al. 2000). Their TF relations are expressed directly in terms of $V_{\rm max}$, estimated mostly from optical rotation curves.

In Fig. A2 also, the TF relation of Giovanelli et al. is the brightest on average. There is very good agreement with the relation of Tully et al., but large differences in slope and/or zero-point (∼0.6 mag) exist in comparison with the other samples.

Part of the differences in zero-point are related to the technique adopted for data analysis. One can derive 'direct' TF relations (least-squares fits minimizing the scatter in magnitude, with logarithmic velocity as an independent variable), 'inverse' TF relations (least-squares fits with magnitude as an independent variable) or bivariate TF relations (as in Giovanelli et al. 1997a). For the same sample, the direct TF relation tends to have a shallower slope, and hence be dimmer at the bright end, than the inverse TF relation (e.g. Willick et al. 1995, 1996). Figs A1 and A2 seem to reveal good agreement between bivariate (Giovanelli) and inverse (Courteau, Tully) TF relations drawn from different samples. The Sakai TF relation is also bivariate; it is steeper than that of Giovanelli et al. but the luminosities are comparable at the high velocity end. Direct TF relations tend instead to be dimmer (MARK III in Fig. A1, top and middle panels; Mathewson in Fig. A2). For the MARK III samples, inverse TF relations are also available (Willick et al. 1995, 1996). In the bottom panel of Fig. A2 we plot the *inverse* MARK III TF relations, also rescaled to a common W_{50} with the TF relation of Giovanelli. There is now better agreement between the luminosities at the bright end.

Various arguments favour an inverse or bivariate fit over a direct fit (Schechter 1980; Tully 1988; Giovanelli et al. 1997a). In this sense

we may disregard the dimmer direct TF relations and consider the relation of Giovanelli et al. to be in reasonable agreement, within uncertainties, with other (bivariate or inverse) TF relations.

APPENDIX B: COLOUR CORRECTIONS TO THE STELLAR M/L RATIO

In this appendix we discuss the relation between the M/L ratio of the stellar (+remnants) component of a galaxy, and its colours – hereinafter the MLC relation. MLC relations are useful, for instance, to colour-correct the TF relation to a common zero-point for all Hubble types, based on the colours of the individual galaxies (Kannappan et al. 2002), or to estimate the radial variation of the stellar M/L ratio in a disc, when deriving the mass profile deconvolving the baryonic and the dark component (Kranz et al. 2003). The luminosities and colours computed here do not include dust effects, hence observational colours and magnitudes should be dust-corrected before our MLC relations can be applied. However, the reddening+dimming effects of dust result in a vector that runs almost parallel to the MLC relation, so that to a first approximation dust has a minor influence on stellar mass estimates from the MLC relation (Bell & de Jong 2001, hereinafter BdJ).

For simplicity, in this appendix we consider only IMFs with the 'standard' mass limits given in Section 3: [0.1–100] $M_\odot$ for the Salpeter, Kroupa and Kennicutt IMFs and [0.01–100] $M_\odot$ for the Larson, modified Larson and Chabrier IMFs (in these cases whether the lower limit is 0.01 or 0.1 $M_\odot$ has negligible impact on the M/L ratios). Other mass ranges, considered for example in Table 2 when tuning the level of metal enrichment, would correspond to simple changes in the zero-point of the MLC relation – as will become apparent from what follows.

Fig. B1 shows some examples of MLC relations for three representative IMFs among those considered in this paper. The plot shows results from our chemo-photometric models of disc galaxies, both the calibrated models in Table 2 and several other models computed during the calibration process. Open symbols represent results for the individual one-zone annuli that constitute our disc models (see Section 6); solid symbols represent results for multizone regions, namely they are the integrated luminosities and colours of the sum of several annuli (e.g. the 'bulge region' within $R < 0.5h_B$, or the 'disc region' $R > 0.5\ h_B$, or the global galaxy, etc.; see Section 6.3). Asterisks represent results for the 'optical disc region' ($0.5 < R < 3\ h_B$) discussed extensively in the paper (Section 6.3). Henceforth, points falling in the same colour–M/L ratio region in the plots result from a variety of star formation and chemical enrichment histories, both one-zone and composite. This is important for seeing whether colours can be good tracers of the underlying M/L ratio variations, with no need of independent knowledge of the star formation and metal enrichment history.

A well-defined linear relation between colour and logarithm of the M/L ratio is apparent in the plots (see also BdJ), at least down to a certain limit in colour (e.g. ∼0.5 in $B - V$); blueward of this, models deviate toward M/L ratios lower (higher in the K band) than the linear fit. In the 'linear range', the MLC relation is rather tight in spite of the variety of SFH and chemical evolution history that can result in a given colour. The worst correlations are obtained with $V - K$, and in general with colours involving the K band ($B - K$, $R - K$, etc.) or in MLC relations involving the K luminosity.

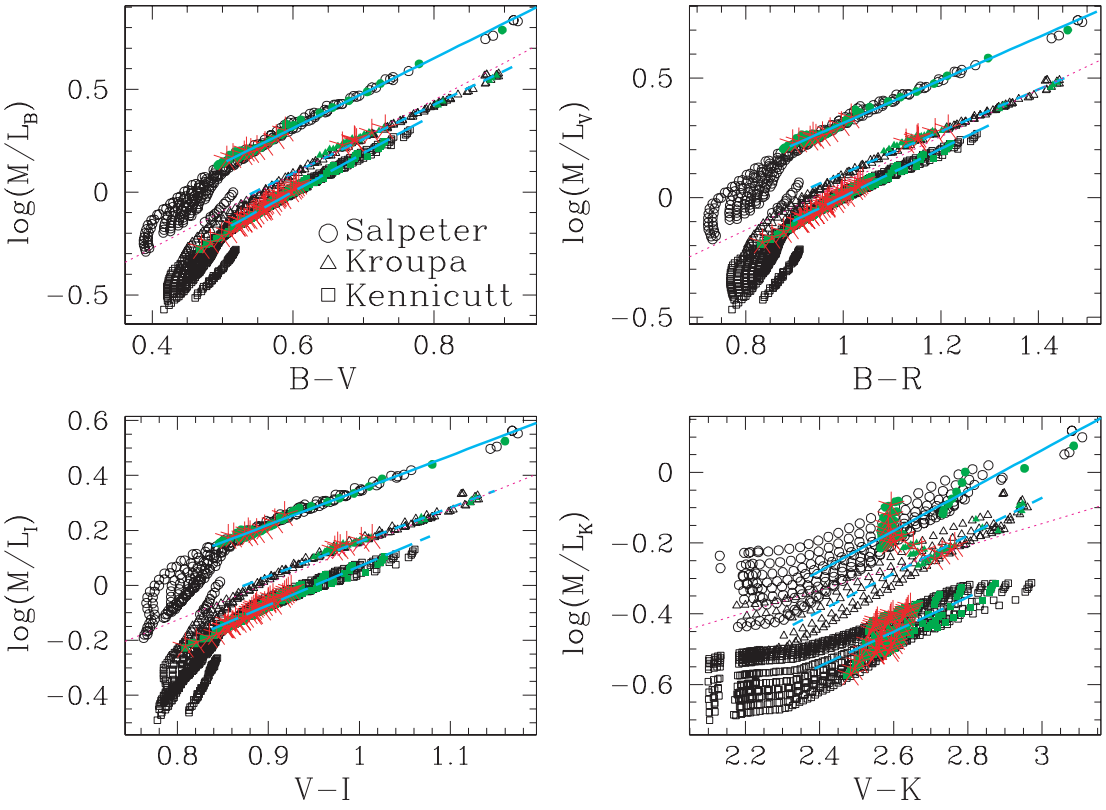

Figure B1. MLC relations from chemo-photometric models of disc galaxies with three representative IMFs. Open symbols, one-zone models for individual disc annuli; solid symbols, multizone models (integrate photometry of bulge region, disc region, or global galaxy); asterisks, 'optical disc' region (see the text). The solid, short dashed and long dashed lines represent the linear fits for the different IMFs, over the respective relevant colour range. The thin dotted line is the linear fit from Bell & de Jong (2001).

The reason is that in optical colours, the age–metallicity degeneracy favours convergence into a tight MLC relation, while in IR bands and colours, age and metallicity effects are less degenerate (see BdJ, their fig. 2 and related comments). Hence the K band (and NIR bands in general) offers the advantage of a smaller variation of the M/L ratio with colour, Hubble type, SFH and metal enrichment history, but colour corrections and MLC relations based on the K band are less tight and compelling.

Fig. B1 shows results for the Salpeter, Kroupa and Kennicutt IMFs as representative cases. To a first approximation, the slope of the MLC relation does not depend on the IMF, which just sets the zero-point; here we confirm the findings of BdJ. For all six IMFs considered in this paper we did verify that, *when the linear fit is performed over the same colour range*, the slope of the MLC relation is independent of the IMF within the uncertainty given by the scatter. We provide in Table B1 the typical, IMF-independent slopes of the MLC relations, and the zero-points corresponding to the different IMFs. We express the zero-points as the logarithmic M/L ratios corresponding to certain values of the colour; specifically:

$$(B-V): \quad \log\left(\frac{M}{L_X}\right) = s_X[(B-V)-0.6]+q_X$$

$$(B-R): \quad \log\left(\frac{M}{L_X}\right) = s_X[(B-R)-1.0]+q_X$$

$$(V-I): \quad \log\left(\frac{M}{L_X}\right) = s_X[(V-I)-0.9]+q_X$$

$$(V-K): \quad \log\left(\frac{M}{L_X}\right) = s_X[(V-K)-2.5]+q_X.$$

Table B1 lists the slope s and zero-point q for the MLC relations in the B, V, R, I, K bands; also given are the colour ranges over which the linear fits are valid. MLC relations with a different colour base (e.g. $V-R$, $B-I$, etc.) can be obtained as a linear combination of these.

The models with the Kennicutt IMF in Fig. B1 do not reach such red colours as the other two sets, because a significant SFR at late times is maintained by the large returned gas fraction from the stellar populations ($1-\alpha = 40$–50 per cent for the Kennicutt, Larson and Chabrier IMFs, Table 3). Consequently, low-b parameters (corresponding to red colours) are hardly achieved with these IMFs, unless gas outflows occur, not included in our disc models. The slopes s_X given in Table B1 have been derived from models with the Salpeter, Kroupa and modified-Larson IMFs, for these models extend to redder colours so the slopes could rely on a wider colour range.

For the Kennicutt (and Larson and Chabrier) case, the linear relation also seems to break down toward the red in $V-K$ (Fig. B1, lower right-hand panel), and in other colours involving the K band ($B-K$, $R-K$, etc.). It is not clear whether this is due to a selection effect – all models with these IMFs are blue in optical colours – or whether it reflects the fact that the evolution of $V-K$ is more sensitive to the IMF than bluer colours (Vazdekis et al. 1996, 1997). Never the less, in such cases we give both lower and upper limits to the 'linear range' where the linear fit can be applied.

A thorough discussion of MLC relations and their implications on the TF relation is given by BdJ. The dotted lines in Fig. B1 are the linear MLC relations derived by BdJ for their favourite set of galactic models (their table 1). Overall, their slopes are in good agreement with ours, albeit slightly steeper (with the exception of the MLC relations in $V-K$). Our slopes are somewhat intermediate between those of their full galactic models (their table 1 and Fig. B1) and those of their simple exponential models at fixed metallicity (their table 4). We impute this slight difference to a tighter calibration in metallicity for our galactic models (Section 6.3), while BdJ select their models mostly on the basis of their K-band magnitude and central surface brightness.

Their normalization of the MLC relation, based on maximal disc arguments, corresponds roughly to a Kroupa IMF. Other IMFs with lower M/L ratios, such as the Kennicutt IMF (Fig. B1), would then imply slightly submaximal discs. The Salpeter IMF seems to be excluded from maximal disc arguments (BdJ).

The deviation from the MLC relation at blue colours seen in Fig. B1 is not apparent in the results by BdJ. However, in their fig. 10 their galactic models with a more regular SFH (their closed box, infall, and outflow case), which are probably more similar to our chemo-photometric models, do show a slight bend-over in the MLC relation and do not stretch to very blue colours. In their favourite set of models, small bursts of star formation are included and the bend-over is wiped out by the larger scatter. The different behaviour

Table B1. Coefficients for the MLC relations. The slopes s_X are independent of the IMF, while the zero-points q_X depend on the IMF. 'Range' indicates the colour range where the linear fit is a good representation of the MLC relation; the lower limit is set by the 'deviations' from a linear relation (see the text and Fig. B1), the upper limit by the reddest colour probed by the models. For the Kennicutt, Larson and Chabrier IMFs, more strict upper limits apply in $V-K$, as indicated (see the text).

Colour	Range	s_B	s_V	s_R	s_I	s_K
$B-V$	0.55–0.90	1.69	1.29	1.11	0.97	0.73
$B-R$	0.95–1.45	1.17	0.89	0.77	0.68	0.51
$V-I$	0.88–1.14	2.17	1.66	1.43	1.26	0.96
$V-K$	2.4–3.0	1.23	0.97	0.84	0.76	0.57
Colour		q_B	q_V	q_R	q_I	q_K
	Salpeter IMF [0.1–100] $M_\odot$					
$B-V$		0.311	0.341	0.317	0.260	−0.115
$B-R$		0.272	0.312	0.292	0.236	−0.134
$V-I$		0.246	0.292	0.275	0.220	−0.147
$V-K$		0.093	0.169	0.168	0.123	−0.222
	Kroupa IMF [0.1–100] $M_\odot$					
$B-V$		0.089	0.120	0.099	0.045	−0.298
$B-R$		0.061	0.099	0.080	0.027	−0.311
$V-I$		0.068	0.104	0.086	0.032	−0.309
$V-K$		0.002	0.048	0.036	−0.015	−0.343
	Kennicutt IMF [0.1–100] $M_\odot$					
$B-V$		−0.002	0.028	0.007	−0.050	−0.421
$B-R$		−0.034	0.004	−0.014	−0.068	−0.435
$V-I$		−0.041	−0.002	−0.020	−0.074	−0.438
$V-K \leqslant 2.8$		−0.182	−0.114	−0.117	−0.162	−0.505
	Larson IMF [0.01–100] $M_\odot$					
$B-V$		0.081	0.111	0.088	0.029	−0.359
$B-R$		0.045	0.085	0.065	0.010	−0.373
$V-I$		0.023	0.068	0.050	−0.004	−0.383
$V-K \leqslant 2.8$		−0.155	−0.075	−0.075	−0.118	−0.466
	Modified Larson IMF [0.01–100] $M_\odot$					
$B-V$		0.064	0.095	0.073	0.016	−0.356
$B-R$		0.031	0.069	0.051	−0.004	−0.371
$V-I$		0.025	0.065	0.047	−0.006	−0.374
$V-K$		−0.123	−0.055	−0.059	−0.104	−0.446
	Chabrier IMF [0.01–100] $M_\odot$					
$B-V$		0.131	0.161	0.138	0.080	−0.303
$B-R$		0.095	0.134	0.115	0.060	−0.318
$V-I$		0.078	0.121	0.103	0.049	−0.325
$V-K \leqslant 2.8$		−0.107	−0.028	−0.029	−0.072	−0.419

toward blue colours is probably due to the fact that, while their models are global galactic models selected so as to have K-band magnitudes and central surface brightnesses representative of spiral galaxies, our blue models (say, bluer than $B - R \sim 0.9$ for instance) corresponds to individual external annuli of our galactic disc models, characterized by overall young ages and low metallicities.

Our steeper slope in the MLC relations in $V - K$ is probably due to the fact that it is defined over a narrower colour range, out of which our MLC relation tends to flatten (Fig. B1, bottom right-hand panel).

Considering that both our galactic chemical evolution models and our population synthesis code differ from BdJ, we regard our results as being in good agreement with theirs, which supports the use of MLC relations as a robust theoretical prediction.

This paper has been typeset from a TEX/LATEX file prepared by the author.